

Published in final edited form as:

*Nat Genet.* 2019 November ; 51(11): 1645–1651. doi:10.1038/s41588-019-0517-5.

## The impact of nonsense-mediated mRNA decay on genetic disease, gene editing and cancer immunotherapy

Rik G.H. Lindeboom<sup>1</sup>, Michiel Vermeulen<sup>1</sup>, Ben Lehner<sup>2,3,4,\*</sup>, Fran Supek<sup>4,5,\*</sup>

<sup>1</sup>Department of Molecular Biology, Faculty of Science, Radboud Institute for Molecular Life Sciences, Oncode Institute, Radboud University Nijmegen, 6525 GA Nijmegen, The Netherlands

<sup>2</sup>Systems Biology Program, Centre for Genomic Regulation (CRG), The Barcelona Institute of Science and Technology, Doctor Aiguader 88, 08003 Barcelona, Spain <sup>3</sup>Universitat Pompeu Fabra (UPF), Barcelona, Spain <sup>4</sup>Institució Catalana de Recerca i Estudis Avançats (ICREA), Passeig Lluís Companys 23, 08010 Barcelona, Spain <sup>5</sup>Institut de Recerca Biomedica (IRB Barcelona), The Barcelona Institute of Science and Technology, 08028, Barcelona, Spain

### Abstract

Premature termination codons (PTCs) can result in the production of truncated proteins or the degradation of mRNAs by nonsense-mediated mRNA decay (NMD). Which of these outcomes occurs can alter the effect of a mutation, with the engagement of NMD depending upon a series of rules. Here, by applying these rules genome-wide to obtain a resource called *NMDetective*, we explore the impact of NMD on genetic disease and approaches to therapy. First, human genetic diseases differ in whether NMD typically aggravates or alleviates the effects of PTCs. Second, failure to trigger NMD is a cause of ineffective gene inactivation by CRISPR-Cas9 gene editing. Finally, NMD is a determinant of the efficacy of cancer immunotherapy, with only frameshifted transcripts that escape NMD predicting a response. These results demonstrate the importance of incorporating the rules of NMD into clinical decision-making. Moreover, they suggest that inhibiting NMD may be effective in enhancing cancer immunotherapy.

---

Nonsense mediated decay (NMD) is a quality control pathway that degrades mRNAs containing premature termination codons (PTCs) because of nonsense or frameshifting mutations<sup>1–3</sup>. However, not all PTCs trigger NMD. For example, PTCs less than 50 nucleotides (nt) upstream of the last exon-exon junction typically do not trigger NMD (‘the

---

Users may view, print, copy, and download text and data-mine the content in such documents, for the purposes of academic research, subject always to the full Conditions of use:[http://www.nature.com/authors/editorial\\_policies/license.html#terms](http://www.nature.com/authors/editorial_policies/license.html#terms)

\* ben.lehner@crg.eu; fran.supek@irbbarcelona.org.

### Data Availability Statement

The NMD efficacy predictions have been made available through the Figshare repository at <https://www.figshare.com/articles/NMDetective/7803398> and via Digital Object Identifier (DOI) at <https://doi.org/10.6084/m9.figshare.7803398>.

### Author Contributions

Conceptualization, FS, BL and RL; Methodology, FS and RL; Formal analysis, RL; Investigation, RL and FS; Validation, RL; Data Curation, RL; Software, RL; Visualization, RL; Writing – Original Draft, FS and BL; Writing – Review & Editing, BL, RL and FS; Funding Acquisition, MV, BL and FS; Supervision, FS, BL and MV.

### Competing Interests

The authors declare no competing interests.

50nt rule')<sup>4</sup>. PTCs in the last exon of a gene were also found not to trigger NMD ('last exon rule')<sup>5,6</sup>. These two 'canonical rules' of NMD have been widely validated<sup>7</sup>, including by analyzing the impact of thousands of inherited human PTCs<sup>8,9</sup> and thousands of PTCs introduced by somatic mutations in human tumors<sup>9,10</sup> on mRNA levels.

Through a large-scale analysis of human cancer exomes and transcriptomes we recently suggested additional 'non-canonical rules' of NMD, e.g. that very long exons (>~400 nt) inhibit NMD ('long exon rule'), a finding supported in subsequent experiments<sup>11</sup>. Moreover, PTCs less than 150 nt from the start codon typically fail to trigger NMD ('start proximal rule'), likely because of translation reinitiation<sup>9</sup>. These rules, and the effect of the distance between a PTC and the wild-type stop codon, and the presence of certain RNA-binding protein motifs, were validated in inherited PTCs and together they explain much of the systematic variability in NMD across genes and mutations in human<sup>9</sup>.

Studies of individual genes have highlighted that NMD can have a strong bearing on human disease phenotypes. In beta-thalassemia, 5' end PTCs in the beta-globin gene, which are seen by NMD, result in a recessive form of the disease, however 3' end PTCs, which escape NMD, result in the dominant form, implying that NMD has protective effects by preventing production of a toxic truncated protein. Conversely, in Duchenne muscular dystrophy, PTCs at the 3' end of the dystrophin gene result in mild phenotypes, while PTCs further upstream are seen by NMD and result in a severe phenotype due to loss of expression of a truncated protein that retains partial activity. NMD can therefore either ameliorate or aggravate diseases<sup>12-14</sup>. PTCs cause a large proportion of human genetic diseases<sup>15</sup>. However, the overall extent to which NMD suppresses or enhances the effects of human genetic disease is unclear<sup>12,16</sup>. This is an important question because drugs that inhibit NMD may represent a general strategy to treat diseases when the production of a truncated protein is beneficial<sup>17-20</sup>.

To evaluate the impact of NMD across diseases we have developed a resource, *NMDetective*, that predicts the effects of PTCs genome-wide in human and mouse. Applying *NMDetective* to known disease mutations reveals that human genetic diseases tend to be often aggravated by NMD. We then use *NMDetective* to show that the efficacy of NMD is an overlooked consideration when performing gene editing using CRISPR-Cas9 and a cause of ineffective gene inactivation. Finally, we apply *NMDetective* to tumor data and show that whether frameshifting mutations do or do not trigger NMD predicts of the efficacy of cancer immunotherapy.

## Results

### A resource for genome-wide prediction of NMD efficacy

To evaluate the impact of introducing PTCs across the human genome, we used rules of NMD learnt from a large-scale analysis of ~10,000 matched tumor exomes and transcriptomes<sup>9</sup>. The NMD efficacy acting on a particular PTC was estimated as the  $-\log_2$  fold-difference in the mRNA level in a tumor sample bearing the PTC, *versus* the median mRNA level in a set of tumors matched by tissue and global gene expression patterns, but with no detectable PTCs in the transcript, as in Lindeboom, et al. <sup>9</sup> (Fig. 1a). Full NMD

efficacy would correspond to a score of 1 (50% decrease in mRNA level due to a heterozygous PTC) and completely inefficient NMD a score of 0 (no change in mRNA level). The genomic features associated with altered NMD efficacy across 2,840 PTCs were incorporated into a predictive model using Random Forest Regression that explained 71% of the systematic variance in NMD efficacy, as estimated on an independent set of 3,151 PTC-inducing frameshifting indel mutations (Fig. 1b; Methods).

We used this model to perform an *in silico* screen of the NMD efficacy of all possible single-nucleotide variants and frameshifting mutations resulting in PTCs in the human and mouse genomes. For the human genome, this produced  $1.2 \times 10^8$  predictions for 101,781 protein-coding transcripts (UCSC Genes, hg38 assembly). Predictions are available as a resource named *NMDetective-A* (Lindeboom, R. G. H.. *NMDetective*. (2019). doi:[10.6084/m9.figshare.7803398](https://doi.org/10.6084/m9.figshare.7803398)).

An analysis of the distribution of NMD efficacy scores (Extended Data Fig. 1a; Methods) suggests that 51% of all possible PTCs in the human genome are predicted to efficiently trigger NMD (*NMDetective-A* score  $>0.52$ ) resulting in destruction of their mRNA transcripts. In addition, 22% of PTCs are predicted not to trigger NMD (*NMDetective-A* score  $<0.25$ ) meaning that their transcripts will not be degraded (the remaining 27% of PTCs have an intermediate NMD efficacy). Thus, whether NMD is triggered or not varies very extensively across possible PTCs in the human genome.

In addition to *NMDetective-A*, which uses Random Forest Regression, we also implemented a simplified predictive model, *NMDetective-B*, that is fully transparent about the series of tests it performs in a decision tree to reach the final prediction about whether a PTC triggers NMD or not (Fig. 1c). The predictive performance of *NMDetective-B* is only slightly lower than that of the Random Forest model (68% versus 71% variance explained on an independent set of PTCs introduced by frameshifting indels; Fig. 1b). *NMDetective-B* therefore provides a reasonable trade-off for situations where interpretability is critical, such as in clinical applications.

*NMDetective-B* consists of four nested tests that incorporate the two canonical rules of NMD as well as two additional rules learnt by analyzing the impact of thousands of PTCs in cancer genomes<sup>9</sup>. The four nested tests in the tree are: (i) if the PTC is in the last exon, (ii) if it is in the last 50 nt of the penultimate exon; (iii) if it is less than 150 nt away from the start codon; and (iv) if it is in a long exon ( $>407$  nt). The four rules in the decision tree were obtained via automated inference from data, without manual adjustment, yet they nonetheless reflect the known mechanistic bases for NMD activity.

All four rules are important for evaluating the impact of PTCs in the human genome. Considering all possible PTCs, 55% are seen by NMD, while others evade NMD: the 'last exon rule' covers 18% of PTCs, the '50nt rule' 3%, the 'start-proximal rule' 12%, and the 'long exon rule' 12% of PTCs (Fig. 1d).

## NMD efficacy impacts the selection on germline variants

Genetic variants that cause severe phenotypes tend to be rare in human populations because they are removed by purifying selection<sup>21,22</sup>. We can therefore evaluate whether NMD contributes to the deleterious effects of PTCs by comparing the allele frequencies of PTCs predicted to trigger and evade NMD. Indeed, 52% of rare PTCs (minor allele frequency,  $MAF = 10^{-6} - 10^{-4}$  in ExAC) are predicted to trigger NMD compared to only 25% of common PTCs ( $MAF > 1\%$ ) and 30% of intermediate frequency PTCs ( $MAF$  between  $10^{-4}$  and  $10^{-2}$ , all differences significant at  $p < 2.2e-12$  by Fisher's exact test; Fig. 2a). Additional tests for selection that account for trinucleotide sequence composition (Supplementary Note, Extended Data Fig. 2a-b) are consistent with NMD frequently modulating deleterious phenotypes resulting from PTCs.

We examined this effect for each of the NMD-evasion rules separately, finding consistent differences between common variants and rare ones for the last-exon and start-proximal rules (Fig. 2a), which are predicted to induce the strongest NMD evasion (Fig. 1c). The effect size for the start-proximal rule (ORs of 1.45 and 1.73 when comparing the relative amount of very rare to intermediate/common PTC variants in different types of NMD regions, respectively) is similar to the one for the well-established last-exon rule (ORs of 1.5 and 2.37), further validating this rule using population genomic data. A cautionary note concerning these analyses is that the observed population variation patterns, which suggest selection on NMD activity, might in part also reflect other types of selection, such as that against longer 3' gene end truncations.

## NMD variably aggravates and alleviates genetic diseases

For germline variants, therefore, the overall impact of NMD is to aggravate the fitness cost of PTCs. This global trend may not, however, apply equally to all genes, as evident in the contrasting examples of the Duchenne muscular dystrophy (*DMD* gene) and the beta-thalassemia (*HBB* gene)<sup>23,24</sup>. To investigate the impact of NMD across different diseases, we evaluated whether clinically-reported PTCs in human disease genes are predicted to trigger NMD. We considered 7,514 nonsense and 12,756 indel variants with clinical significance (having ClinVar assertions) in 752 genes causing genetic disorders for which more than five PTC variants were available.

The direction of the effect of NMD is variable across genes and diseases (Extended Data Fig. 1b): in total, 49 disease genes were more than 2-fold enriched for pathogenic PTCs predicted to evade NMD. An excess of pathogenic PTCs in NMD-evading regions suggests that NMD reduces the pathogenicity of PTCs that it can detect and thus that NMD alleviates the phenotype (illustrated in Extended Data Fig. 1c). However, when considering the converse case, 155 disease genes were more than 2-fold enriched for pathogenic PTCs that trigger NMD. This predominance of genes where pathogenic PTCs tend to trigger NMD (155 versus 49,  $P = 5.1e-14$  by sign test) suggests that, globally, NMD tends to more commonly aggravate rather than ameliorate the effects of genetic diseases.

When examining individual genes, we found 17 disease associated-genes significantly enriched for PTCs that trigger NMD and 13 significantly enriched for PTCs that do not

trigger NMD (Fig 2b-c; False Discovery Rate (FDR) <5%; this increases to 35 and 40 genes, respectively, at FDR<25%, Extended Data Fig. 3c-d). Similar results were observed when normalizing to local density of missense variants (Extended Data Fig. 3a-b, Supplementary Note). This indicates that NMD affects the severity of phenotypes in these heritable diseases.

Examples of disease genes where the enrichments suggest that NMD aggravates the disease (Extended Data Fig. 3c) include multiple tumor suppressor genes (76-fold enrichment, FDR=2.6e-10), consistent with mutations in these genes acting via a loss-of-function mechanism that would be intensified by NMD. Besides tumor suppressors, other examples include the genes *JAG1*, *DYRK1A* and *ZIC2*, which have all been reported to cause disease though haploinsufficiency<sup>25-27</sup>. For these cases, drugs that inhibit NMD or that cause stop-codon read-through may alleviate disease severity<sup>28,29</sup>. For example, an inhibitor of NMD can restore levels of P53 protein and the expression of its downstream targets, causing cell death in cells that bear NMD-triggering PTCs in *TP53*<sup>30</sup>.

There are, however, multiple diseases where we predict that NMD alleviates the phenotype (discussed in Supplementary Note; Extended Data Fig. 3d). In these cases inhibiting NMD would not have a favorable impact.

These analyses show that NMD commonly modulates the severity of phenotypes resulting from PTCs. We therefore hypothesized that considering NMD rules can improve pathogenicity predictions of PTCs (Supplementary Note). Indeed, including the NMD rules in a joint model with known predictors of pathogenicity significantly improves the prediction after all other features are controlled for (Fig. 2d-e). This suggests that NMD rules should be included in statistical models that predict variant pathogenicity.

### **NMD efficacy determines the outcome of gene editing**

CRISPR-Cas9 and related gene editing technologies have become widely adopted for gene inactivation and offer great promise for the treatment of genetic diseases<sup>31</sup> and for high-throughput genetic screens<sup>32-36</sup>. The mutations introduced by Cas9 are most often frameshifting indels<sup>37</sup>. These frameshifts can result in PTCs that will either result in mRNA degradation by NMD or the production of truncated proteins, depending upon whether NMD is triggered or not (Extended Data Fig. 1c). Both scenarios can be used as loss-of-function models<sup>2</sup>, but degradation of mRNA is desirable because of partial rescue and gain-of-function effects that may result from truncated proteins.

To systematically evaluate the importance of NMD for gene inactivation by gene editing, we made use of a dataset where tiled sgRNAs were used to target nine genes encoding human and mouse cell surface markers<sup>36</sup>. In all eight multi-exon genes we found higher protein levels, suggestive of reduced NMD efficiency, if the sgRNA sites were located in the 3' ends of the coding sequence in regions that evade NMD by the last-exon or the 50nt rule (Fig. 3a; difference 2.4-fold and 2.5-fold, respectively, normalized to NMD-detected regions of a gene). There is a certain diversity of effect sizes across these eight genes (Extended Data Fig. 4c; interquartile range, IQR, 1.5-fold to 5.0-fold for the last-exon rule. The start-proximal and the long-exon NMD rules are also associated with higher protein levels in this dataset (Supplementary Note). Furthermore, analysis of saturation editing of the BRCA1

gene<sup>35</sup> validates that the first 150 nt of the coding region are not well suited for gene inactivation by CRISPR-Cas9 (Fig. 3c; Extended Data Fig. 5b-e, Supplementary Note).

To further substantiate these findings, we analyzed the data from a genome-wide CRISPR screen for gene essentiality<sup>32</sup>. Here we contrasted the sgRNAs targeting different regions of each gene for their ability to produce a fitness defect in essential genes<sup>32</sup>. sgRNAs targeting regions covered by each of the four NMD evasion rules were highly significantly associated with increased cell fitness (Fig. 3b).

For the last exon rule there was a 38% reduced sgRNA depletion in essential genes, compared to NMD-trigger regions ( $p < 2e-16$  by two-tailed Mann-Whitney U test). For the 50nt rule there was a 12% reduction ( $p = 8e-5$ ) and for the long exon rule there was a 31% reduction ( $p < 2e-16$ ). Finally, the same held true for the start-proximal rule, which had a larger effect in the cases where there is an in-frame downstream AUG (20% reduction,  $p = 2e-12$ ) than when the downstream AUG is out-of-frame (9% reduction,  $p = 2e-4$ ), further supporting re-initiation of translation as a common mechanism by which a 5' PTCs evade NMD<sup>9</sup>.

Importantly, the effect size for the non-canonical long exon rule is similar to the established last exon rule (31% vs 38% reduced sgRNA depletion), and the effect size for the non-canonical start-proximal rule is larger than for the canonical 50nt rule (20% vs 12%), underscoring the importance of the two non-canonical rules for governing NMD efficacy. In a set of known non-essential genes, there was no loss of fitness, irrespective of the NMD rules (Extended Data Fig. 5a). The above observations validated in two additional genome-wide CRISPR screen studies for gene essentiality<sup>33,34</sup> (Extended Data Fig. 6). Accounting for NMD rules improves predictions of sgRNA efficacy: NMD-triggering sgRNAs can distinguish essential from non-essential genes at an AUC=0.90, while this is reduced for NMD-evading sgRNAs (AUC=0.74-0.88 for different NMD-evasion rules; Extended Data Fig. 4b).

Lastly, these CRISPR screen data also support additional non-canonical determinants of NMD efficacy<sup>9</sup>. In particular, we observed reduced NMD efficacy when the distance to the downstream exon junction or to the end of the coding region is long, or when mRNAs that have shorter half-lives are targeted (Extended Data Fig. 6), consistent with competition between NMD and other mRNA turnover processes.

### **Only frameshifts not detected by NMD predict the response to immunotherapy**

In recent years, immune checkpoint inhibitors have demonstrated remarkable efficacy in a subset of cancer patients<sup>38</sup>. A robust predictor of the response to immunotherapy is the overall tumor mutation burden, presumably because it reflects the propensity to generate neo-antigenic peptides that can be detected by the immune system<sup>39,40</sup>. The mutations most strongly associated with immunotherapy response are small indels<sup>41</sup>, consistent with indels resulting in the production of frameshifted peptides with aberrant amino acid sequences. However, frameshifts also usually introduce PTCs and so can trigger NMD. We hypothesized therefore that NMD may modulate the efficacy of cancer immunotherapy and



specifically that only the burden of frameshifts that do not trigger NMD will predict clinical response.

Indeed, in a pan-cancer cohort we find that the burden of frameshifts that do not trigger NMD correlates with tumor immune reactivity (Extended Data Fig. 7-8; Supplementary Note). The enhanced immunoreactivity of tumors carrying frameshifting mutations that escape NMD suggests that these tumors may also respond better to immunotherapy. To test this, we collated five datasets of tumor exomes paired with patient response data: melanoma (treated with PD-1 and CTLA-4 inhibitors)<sup>42,43</sup>, renal cancer (anti-PD-1)<sup>44</sup>, lung cancer (anti-PD-1)<sup>45</sup>, and an additional set with diverse cancer types and treatments<sup>46</sup>. We stratified the patients into responders and non-responders (Methods) and compared their frameshifting indel burden separately for regions predicted by *NMDetective* to trigger or evade NMD.

In four out of five studies, the responders had a significantly higher number of frameshifts predicted not to trigger NMD than the non-responders (1.5 - 4.3 fold higher in responders compared to non-responders,  $p=0.007-0.017$ , one-tailed Mann-Whitney U test; Fig 4a). In the fifth study there was a trend in the same direction ( $p=0.075$ ), giving a pooled  $p$ -value of  $1.5 \times 10^{-5}$  in a meta-analysis across the studies (Fisher's method for combining  $p$ -values) and a mean 2.4-fold difference in burden of NMD-evading frameshifts.

In contrast, when examining frameshifts predicted by *NMDetective* to trigger NMD, there was no association with the response to immunotherapy in any study ( $p=0.129-0.666$ ) or overall (meta-analysis  $p=0.641$ ; Fig 4a). The average number of somatic frameshifts per patient that were predicted to trigger NMD or not was similar (Fig 4a). The above results broadly hold regardless of whether the frameshifts are classified by the location of the frameshifting indel (Fig. 4a) or by the location of the proximal downstream PTC caused by the frameshift (Extended Data Fig. 9a).

The NMD-evading frameshifts classified by all four rules were enriched in responders (Fig. 4b) and were most commonly covered by the last exon rule (49%), followed by the long exon rule (33%), and the non-canonical start-proximal rule (12%; Fig. 4c), demonstrating the importance of the complete set of NMD rules in *NMDetective*.

In a joint predictive model that classifies responders *versus* non-responders, the NMD features have a substantial contribution to predictive ability (Supplementary Note; Extended Data Fig. 9b,c). We register an increase by 5.86% of the fraction of patients correctly classified in a model which considers tumor mutation burden (TMB) and NMD-evading frameshifts, compared to a TMB-only baseline ( $p=0.003$ ; Extended Data Fig. 9d). The area under the precision-recall-curve increases from 0.55 (TMB-only) to 0.63 (TMB + NMD-evading frameshifts).

Taken together, these analyses provide strong evidence that, by preventing the expression of neoantigens, NMD reduces the efficacy of cancer immunotherapy.

## Discussion

We have shown here that the activity of the NMD pathway is of broad importance for selection on germline variants, disease phenotypes, gene editing efficacy, and the immune reactivity of tumors. *NMDetective* is a comprehensive resource containing predictions for whether PTCs occurring at any location in the human and mouse genome will trigger NMD.

Overall, NMD tends to aggravate phenotypes for many PTCs, suggesting that pharmacological NMD inhibition may be a broadly applicable strategy for curbing the progression of many genetic diseases<sup>17–20</sup>. Inhibitors of NMD have been developed and are well tolerated<sup>29,30,47,48</sup>. However, knowing the causal mutation for each patient and whether it triggers NMD will be crucial for targeting therapies to patients who will benefit.

We also further validate the non-canonical NMD rules previously discovered in our large-scale analysis of cancer genomes<sup>9</sup>. Both population allele frequencies and gene editing by CRISPR-Cas9 validate that start-proximal PTCs and PTCs in long exons do not efficiently trigger NMD. These non-canonical NMD rules cover a substantial proportion of the human coding genome and are similarly important for predicting the efficacy of NMD as the canonical rules (Fig. 1). For gene editing in particular, the tendency of sgRNA design algorithms to target the first 150 nts of coding sequence needs to be revised, as frameshifts in these regions often fail to trigger NMD and so can result in incomplete gene inactivation.

Finally, we suggest that NMD suppresses both the immune reactivity of tumors and their response to immunotherapy. Remarkably, only those frameshifting indels that evade NMD were associated with a response to immune checkpoint inhibitors. Together with the enhanced immune reactivity of tumors with mutations in the NMD pathway, this suggests that inhibiting NMD may be an effective strategy to potentiate the efficacy of checkpoint inhibitors<sup>18,49</sup>. By preventing the destruction of PTC-containing transcripts, reduced NMD activity may enhance the expression of neo-antigens and so the efficacy of immunotherapy.

## Methods

### Predicting NMD efficacy

The fold-change in mRNA abundance of PTC-bearing transcripts was used to quantify NMD efficacies as described in Lindeboom, et al.<sup>9</sup>. In short, after stringent filtering to exclude genome segments with copy-number alterations, we identified 2,840 high-confidence nonsense mutations in the dominant transcript<sup>50</sup> of 1,900 protein-coding genes in 9,769 tumor samples with matched exome and transcriptome data in the TCGA Data Portal (superseded by NCI Genomic Data Commons<sup>51</sup>). Next, we compared the mRNA abundance (as TPM, after filtering by a principal components analysis as in Lindeboom, et al.<sup>9</sup>) of each PTC-bearing transcript to the median expression of the same transcript in similar tumor samples (defined by tumor type and further subdivided by non-negative matrix factorization clustering on global gene expression patterns), but where PTCs were absent. Finally, the  $-\log_2$  fold-difference in TPM was then used to quantify NMD efficacy acting upon each PTC. We used these NMD efficacy scores derived from cancer transcriptomes as a training set to derive the *NMDetective* predictive models. Such models were then used to make



genome-wide predictions for all possible PTC variants, based on genomic features we found to be associated with NMD efficacy acting on observed PTC mutations, and additionally requiring that these features validated in an independent set of somatic frameshifting indels and also in a set of germline PTC variants<sup>9</sup>.

The *NMDetective-A* resource was generated using Random Forest regression (*randomForest* package version 4.6-14 in R), while the *NMDetective-B* resource was based on a decision tree model using a conditional inference tree algorithm (*party* package version 1.3-1 in R). Both models were trained on NMD efficacy scores, while using the following predictive features: *on\_last\_exon* and *in\_last\_50nt\_of\_penultimate\_exon* as boolean features, with *rna\_halflife* quantified in minutes and with the following features quantified in number of nucleotides: *distance\_to\_coding\_start*, *exon\_length*, *distance\_to\_downstream\_EJC* and *distance\_to\_wildtype\_stopcodon*. The 3'UTR was not included when calculating the exon length of the last exon, and the *distance\_to\_coding\_start* was capped at 1000 nt. RNA half-life values were taken from Friedel, et al.<sup>52</sup> and missing values were imputed with the median RNA half-life (which was 300 minutes). The distance to downstream EJC was calculated from the presumed 5' border of the EJC, located 50 nt from the exon junction. An additional feature that was included in the training data set was the variant allele fraction (VAF) of each somatic PTC variant; in order to obtain the predictions in the *NMDetective-A/B* resources, the median VAF values in the training data were supplied to the models.

The *NMDetective-A* efficacy scores were clustered by a univariate gaussian mixture model on all hg38 scores. Expectation maximization by the *flexmix* package version 2.3-15 in R was performed for 1,000,000 iterations at a tolerance of 1e-15, testing 1 to 15 clusters to determine optimal amount of clusters (determined with the bayesian information criterion). This resulted in 5 clusters and the clusters with the two highest, the two intermediate, and the lowest mean NMD efficacy scores were classified as efficient, intermediate and inefficient NMD efficacy clusters, respectively.

Random Forest regression was performed with 100,000 trees and the amount of variables sampled at each split set to one. Only splits significant at a permutation-based P value < 0.05 were selected for the final decision tree model. The performance of both models reported in Fig 1b was assessed using an independent test set with NMD efficacies of 3,151 PTC-introducing frameshift mutations<sup>9</sup>, thus obtaining the R<sup>2</sup> values which were adjusted to account the maximum attainable R<sup>2</sup> given the reproducibility of the measurements (correction for attenuation; see Lindeboom, et al.<sup>9</sup>).

Unless stated differently, downstream analyses were performed by using the *NMDetective-B* NMD efficacy predictions on the UCSC knownGene databases downloaded in January 2018<sup>53</sup>, after excluding genomic regions with multiple NMD efficacy scores because of isoforms or overlapping genes.

The data deposited at Lindeboom, R. G. H.. *NMDetective*. (2019). doi:[10.6084/m9.figshare.7803398](https://doi.org/10.6084/m9.figshare.7803398) contains *NMDetective-A* and *NMDetective-B* efficacy scores for all possible single-nucleotide variants and out-of-frame indel mutations that introduce PTCs in (UCSC

knownGene) protein coding transcripts of recent versions of the human and mouse genome (hg19, hg38, mm9 and mm10).

### Disease genetics

Release 1.0 of the Exome Aggregation Consortium<sup>54</sup> (ExAC) was used to analyze the signatures of selection acting on nonsense mutations. Variants with clinical significance were taken from the ClinVar database version 20170905<sup>55</sup> on genome build GRCh37. Common nonsense mutations (allele frequency > 0.001) in ExAC were selected as benign mutations and compared to known pathogenic nonsense mutations in ClinVar to train and test a logistic model that separates benign and pathogenic variants based on ALoFT<sup>56</sup> features and on our NMD prediction. Only the selection of ALoFT features shown in Fig. 2e were used to predict pathogenic mutations, removing features that were redundant or that could be confounded with our NMD rules (for example distance to start- and stop-codon). Features describing protein domains and post-transcriptional modifications were described by a binary variable for every feature with the test if the variant intersected with a domain or modification. The ALoFT sequence conservation feature was quantified as dN/dS ratios compared to mouse.

To test for significant differences in density of clinically relevant PTCs in NMD-evading regions of individual genes, we used all nonsense and frameshift mutations in ClinVar and focussed only on genes with at least five PTC introducing variant. The largest UCSC knownGene transcript per gene was selected for analysis. For every gene, we compared the PTC density in individual NMD regions, and in all NMD evading regions combined, to the PTC density in the NMD-detected part of the gene. To control for potential effects of mutation hotspots and amount of ClinVar entries per gene, we also compared ClinVar PTCs to rare missense mutation density in ExAC (allele frequency < 0.001) in Extended Data Fig. 3a-b.

To control for a possible bias in sequence properties of germline variants in different types of NMD regions, we used the trinucleotide context of all germline variants reported in the whole-genome gnomAD release 2.1.1<sup>57</sup> to determine sequence and VAF dependent substitution probabilities. We used these probabilities to simulate mutations at different VAF ranges and filtered for PTC-introducing variants to test for differences in their distribution over different types of NMD regions.

### CRISPR-Cas9 gene inactivation efficiency

We used genome-wide CRISPR screen data from Wang, et al.<sup>32</sup>, to test if NMD evasion affects the knock-out efficiency of essential genes presented in Fig. 3b (18166 genes targeted, ~10 sgRNAs per gene). Similar data from Meyers, et al.<sup>33</sup> and Wang, et al.<sup>34</sup> and was used as validation datasets and presented in Extended Data Fig. 6a-e. In all three studies, cancer cell lines were grown for several doublings after being transduced with a genome-wide sgRNA library, and the depletion of sgRNAs in the population was used to identify essential genes. To calculate the fold change in sgRNA abundances shown in Fig. 3b, we normalized the read counts by total sequencing depth and added 0.001 to every read count value. Essential gene definitions used in Fig 3b were taken from the corresponding

study, for every cell line separately at  $FDR < 5\%$ . Genes with a short half-life ( $< 5$  hours) were not shown in Fig. 3b, but were included in Extended Data Fig. 5a. In Extended Data Fig. 6, we averaged the fold change for each sgRNA within each study, and show only sgRNAs that target a gene that was a significant essential gene in at least one cell line in Wang, et al.<sup>32</sup> at  $FDR < 5\%$ .

To quantify how well the depletion of sgRNAs in different types of NMD regions can predict essential genes, we used the log transformed fold change of individual sgRNAs from Wang, et al.<sup>32</sup> to predict curated essential and non-essential genes from Hart and Moffat<sup>58</sup>. Saturation genome editing data by CRISPR of the BRCA1 gene was taken from Findlay, et al.<sup>35</sup>. Here, BRCA1 mRNA and genome sequencing in saturation genome-edited HAP1 cells was performed to quantify the mRNA expression of PTC-introducing SNVs, normalized to their abundance in the genomic DNA (yielding the RNA score). We used these RNA scores to investigate if NMD evasion affected the expression of PTCs introduced by CRISPR.

Data from a CRISPR screen tiling genes encoding three human and six mouse cell surface proteins, in which protein knock-out efficiencies were determined by flow cytometry was obtained from Doench, et al.<sup>36</sup>. We used blastn<sup>59</sup> version 2.2.28+ to align sgRNA target sequences to the hg19 or mm9 genome to obtain the genomic target site, and only selected sgRNAs with a perfect match to the targeted genes. Read counts for sgRNAs were normalized for total sequencing depth, and for every cell surface protein we compared the mean normalized read counts from the negative population to the unsorted population. We only considered genes that were targeted by more than 50 sgRNAs and where the mean fold change in sgRNA abundance differed from the unsorted population by  $> 25\%$ . For every targeted gene, we show the isoform that was targeted by most sgRNA matches.

To identify appropriate CRISPR design tools to investigate the distribution of affected NMD rules by sgRNAs designed for CRISPR knock out experiments, we focused on highly used tools that allow for batch submission of target genes. We therefore used the CRISPR design tools E-CRISP<sup>60</sup> and 'CRISPRko' offered by the Genetic Perturbation Platform of the Broad Institute, to design sgRNAs for knock-out experiments of the top 100 most cited genes (from <http://doi.org/10.5281/zenodo.1066066>).

### Tumor immune reactivity

Somatic mutation data detected by the MuTect2 algorithm from tumor samples in the TCGA program were downloaded on 3 October 2017 from the GDC Data Portal<sup>51</sup>. Predicted immunogenomic features were taken from Thorsson, et al.<sup>61</sup>. RNA expression of immune checkpoint related genes shown in Extended Data Fig. 7 were downloaded using the R package RTCGA version 1.12.0.

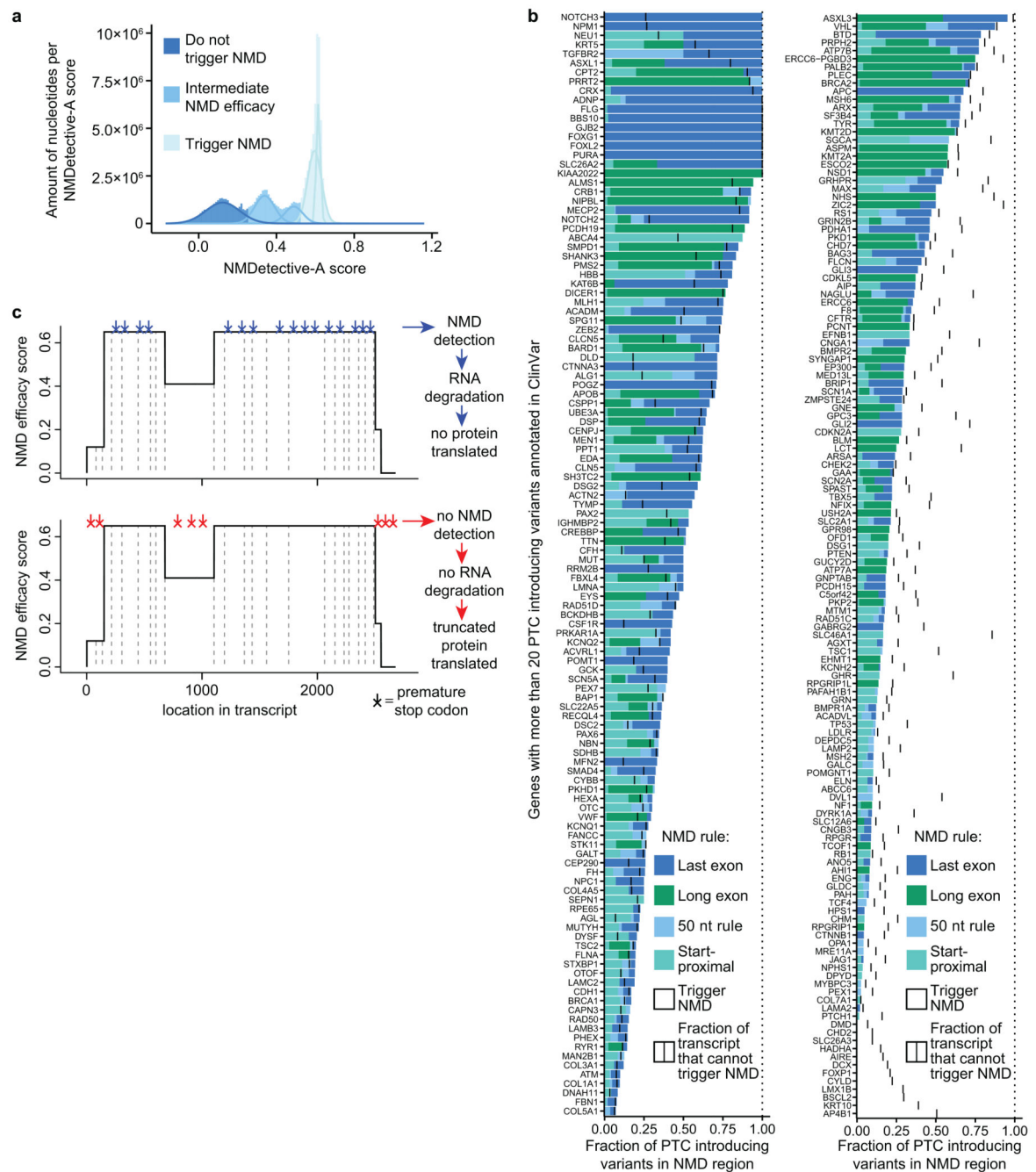
We gathered whole exome sequencing (WES) data of pretreatment tumor samples from patients receiving immune checkpoint blockade drugs from five different studies<sup>42–46</sup> (273 patients in total). Most patients were stratified by response evaluation criteria in solid tumors<sup>62</sup> version 1.1 (RECIST 1.1), with the exception of patients in Hugo, et al.<sup>43</sup>, who were classified by irRECIST<sup>63</sup>. We classified patients in response or no-response groups

based on information supplied by the authors of the respective studies. Patients were classified as responders based on the following information: in Miao, et al.<sup>44</sup> patients with ‘clinical benefit’ or ‘intermediate benefit’ as responders, in Van Allen, et al.<sup>42</sup>, Miao, et al.<sup>46</sup> and Hugo, et al.<sup>43</sup> patients with ‘response’, and in Forde, et al.<sup>45</sup> patients with ‘major pathological response’. Patients in the studied cohorts received the following immune checkpoint blockade drugs: Van Allen, et al.<sup>42</sup> were metastatic melanoma samples and received ipilimumab (anti CTLA-4), Hugo, et al.<sup>43</sup> were melanoma samples that received pembrolizumab and nivolumab (anti PD-1), Miao, et al.<sup>44</sup> contained metastatic clear cell renal cell carcinoma samples that received nivolumab, Forde, et al.<sup>45</sup> were advanced non-small-cell lung carcinoma samples that received nivolumab. Miao, et al.<sup>46</sup> included tumor samples originating from bladder, lung, skin and head/neck, which were treated with anti PD-1, anti PD-L1, and anti CTLA-4 drugs. Because Miao, et al.<sup>46</sup> presented a collection of previously published samples together with some new WES samples, care was taken in selecting the WES samples unique to this study. To count the number of frameshifts that cannot trigger NMD, we used the indel variants supplied by the authors and aligned them to NMD efficacy scores on the canonical transcript database of UCSC, and counted the frameshifts in any of the NMD rules as frameshifts that do not trigger NMD. The tumor mutational burden (TMB) was defined as the total amount of SNVs in a tumor sample.

### Statistics

All statistical analyses were performed in R version 3.4.4. The statistical tests applied are described in the corresponding section. Unless stated differently, a two-tailed Mann-Whitney U test was used. A Life Sciences Reporting Summary accompanies this article.

### Extended Data

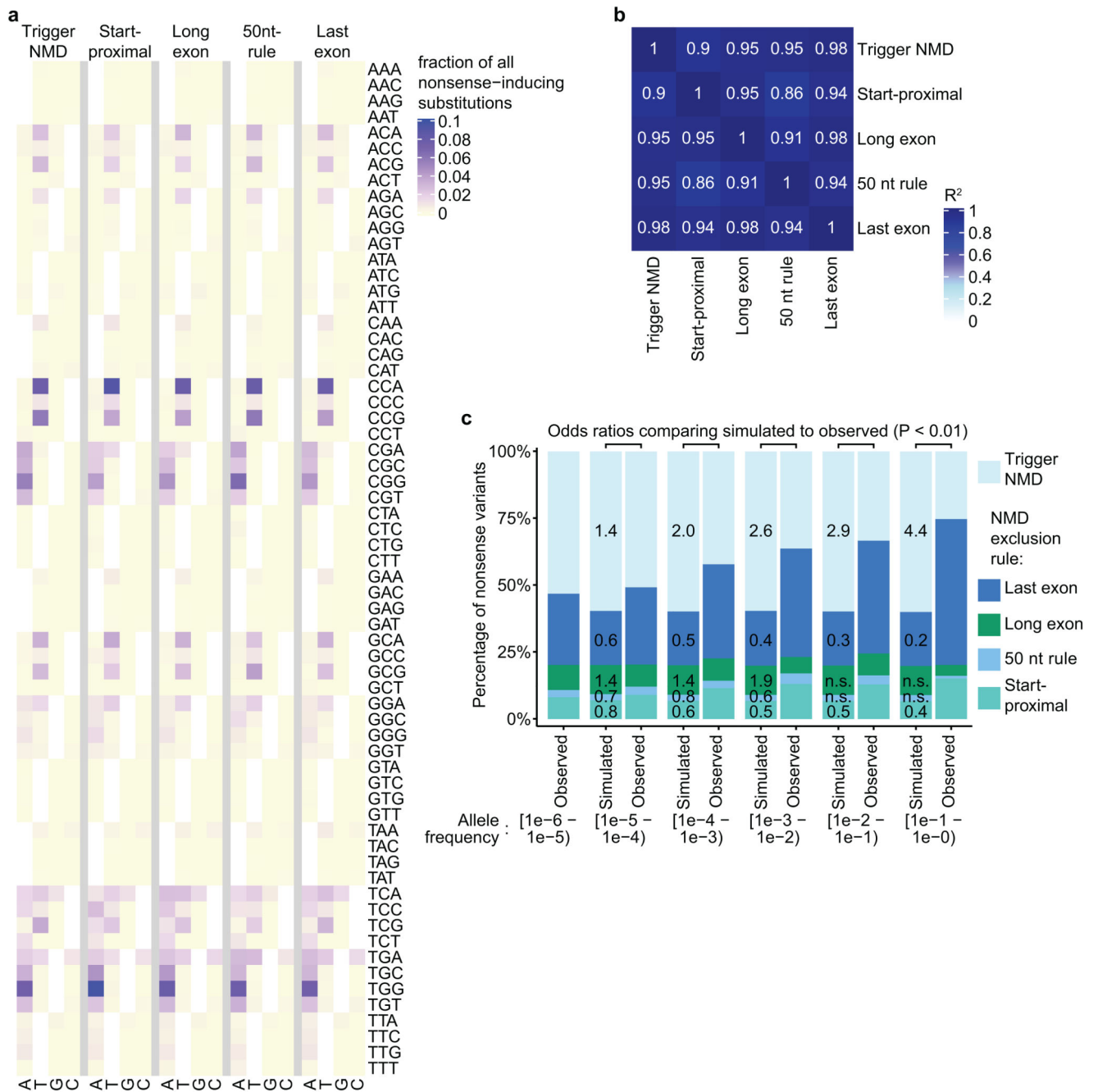


**Extended Data Fig.1. The distribution of genome-wide NMD efficacy scores and of NMD rules in all genes with more than 20 disease-associated PTC variants.**

**a**, the distribution of NMDetective-A scores over all genes in hg38 reveals three global clusters of inefficient, intermediate-efficiency and efficient NMD. **b**, genes in which there is an excess of PTCs in NMD-evading regions (left barplot) and genes where there is a dearth of PTCs in NMD-evading regions (right barplot). The proportion of PTCs in different NMD-evading regions is shown as colored segments in the bar chart. The relative portion of the protein-coding mRNA sequence that is covered by the NMD rules is shown as a black

vertical stripe. **c**, a schematic of a gene that illustrates how PTCs that trigger or evade NMD can lead to different outcomes in protein expression.

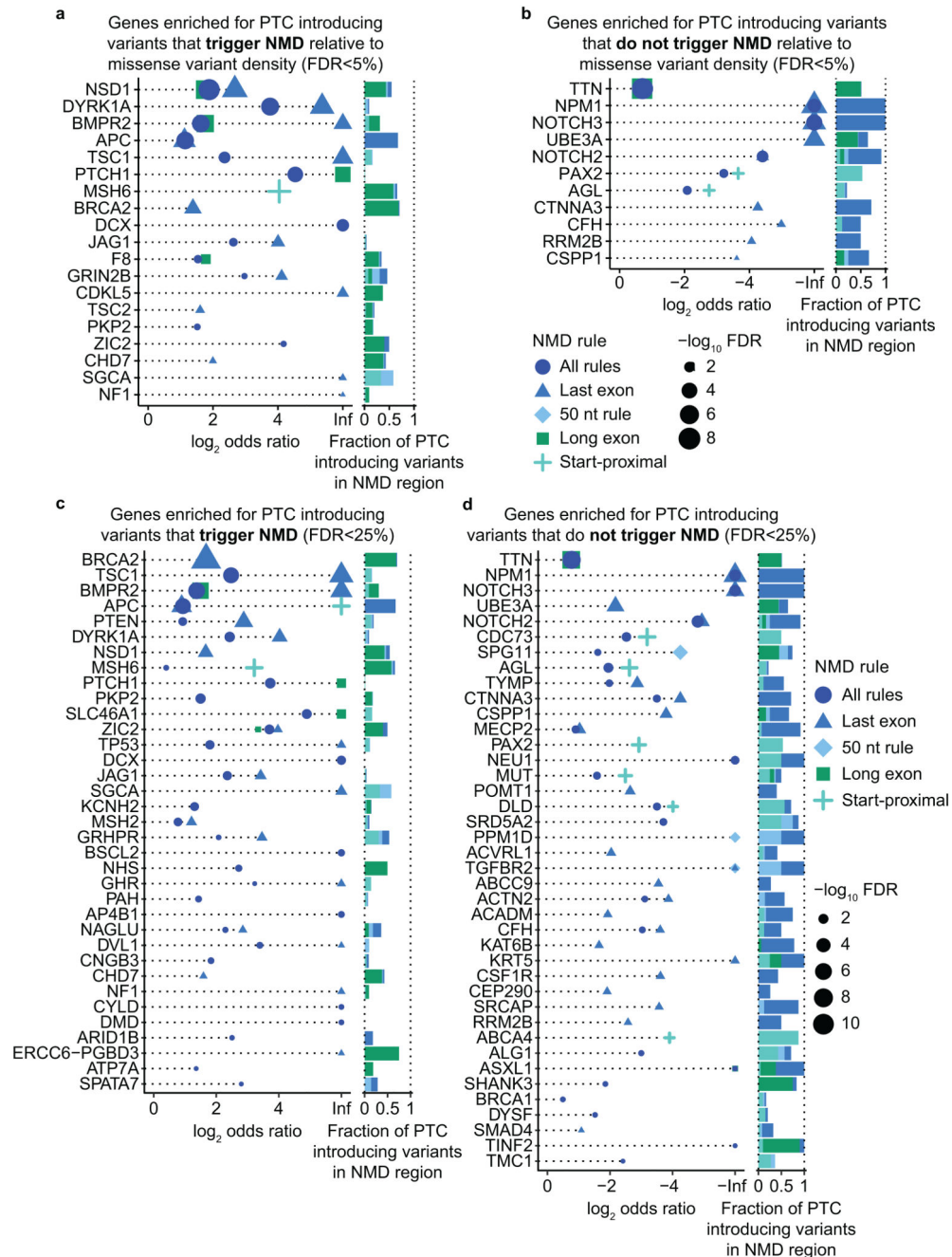




**Extended Data Fig.2. The sequence context of nonsense variants is not different between different types of NMD regions.**

**a**, the trinucleotide spectrum of nonsense variants in ExAC is consistent across gene regions that trigger or evade NMD, **b**, spectrum of variants shows high Pearson correlations between the different types of NMD regions. **c**, the baseline NMD-evasion rule coverage for population genomic data, obtained from nonsense variants simulated from the trinucleotide context of whole-genome population variants at different VAF ranges, exhibits a consistent distribution at different VAF ranges. Observed nonsense variants are increasingly enriched

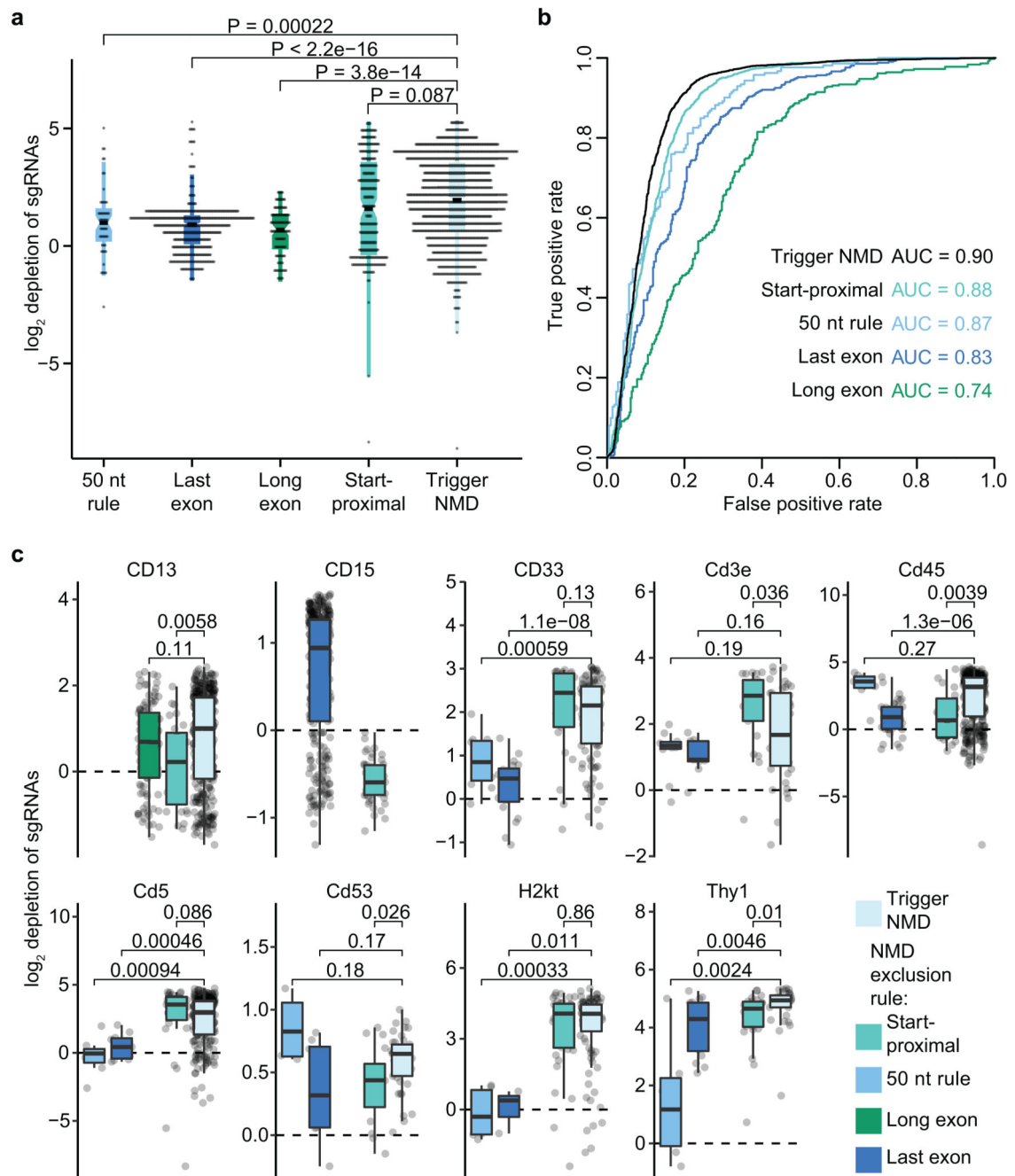
towards NMD-evading regions with an increasing VAF, compared to the simulated baseline at same VAFs. Odds ratios significant at  $P < 0.01$  (Fisher's exact test) are shown, comparing the distribution of simulated *versus* observed nonsense mutations.



**Extended Data Fig.3. Disease genes with a significant enrichment of PTC variants that do or do not trigger NMD, with and without normalization to local density of missense mutations.**

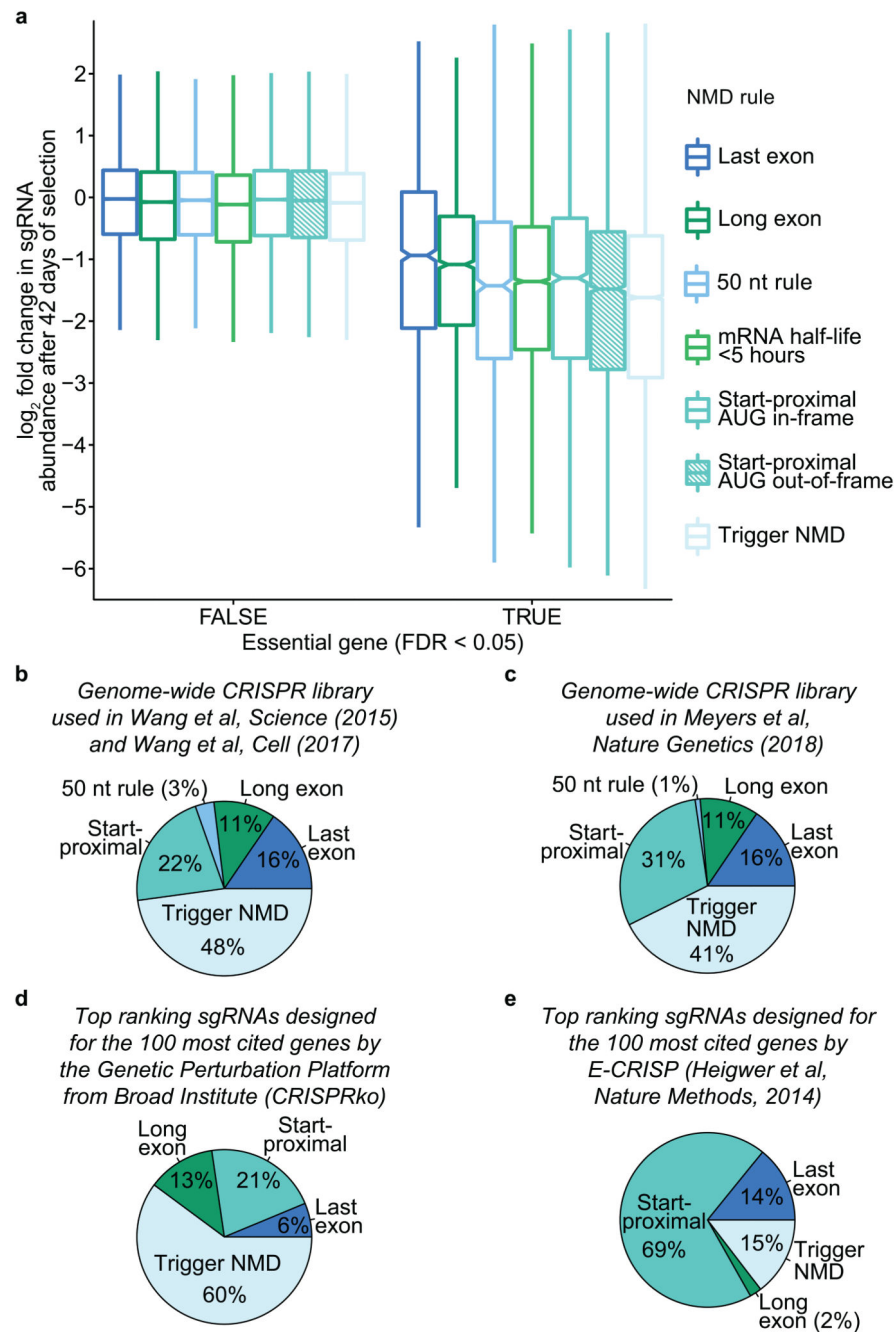
**a-b**, significant enrichment of genes at FDR<0.05 after normalization to the number of ClinVar missense variants observed in the same NMD regions. **c-d**, genes significant at an FDR<25% are shown (see Fig. 2d-e for a list at FDR<5%). Log<sub>2</sub> odds ratios are for ClinVar frequencies of NMD-evading frameshifting indel and nonsense variants versus NMD-detected frameshifting indel and nonsense variants regions of a gene, normalized to the length of the NMD-evading versus NMD-detected regions. FDRs are by Fisher's exact test,

two-tailed, Benjamini-Hochberg adjusted. **a-d**, log<sub>2</sub> odds ratios are shown separately for the four rules, for each rule which is significant in a particular gene.



**Extended Data Fig.4. Effect of NMD rules observed in CRISPR assays.**

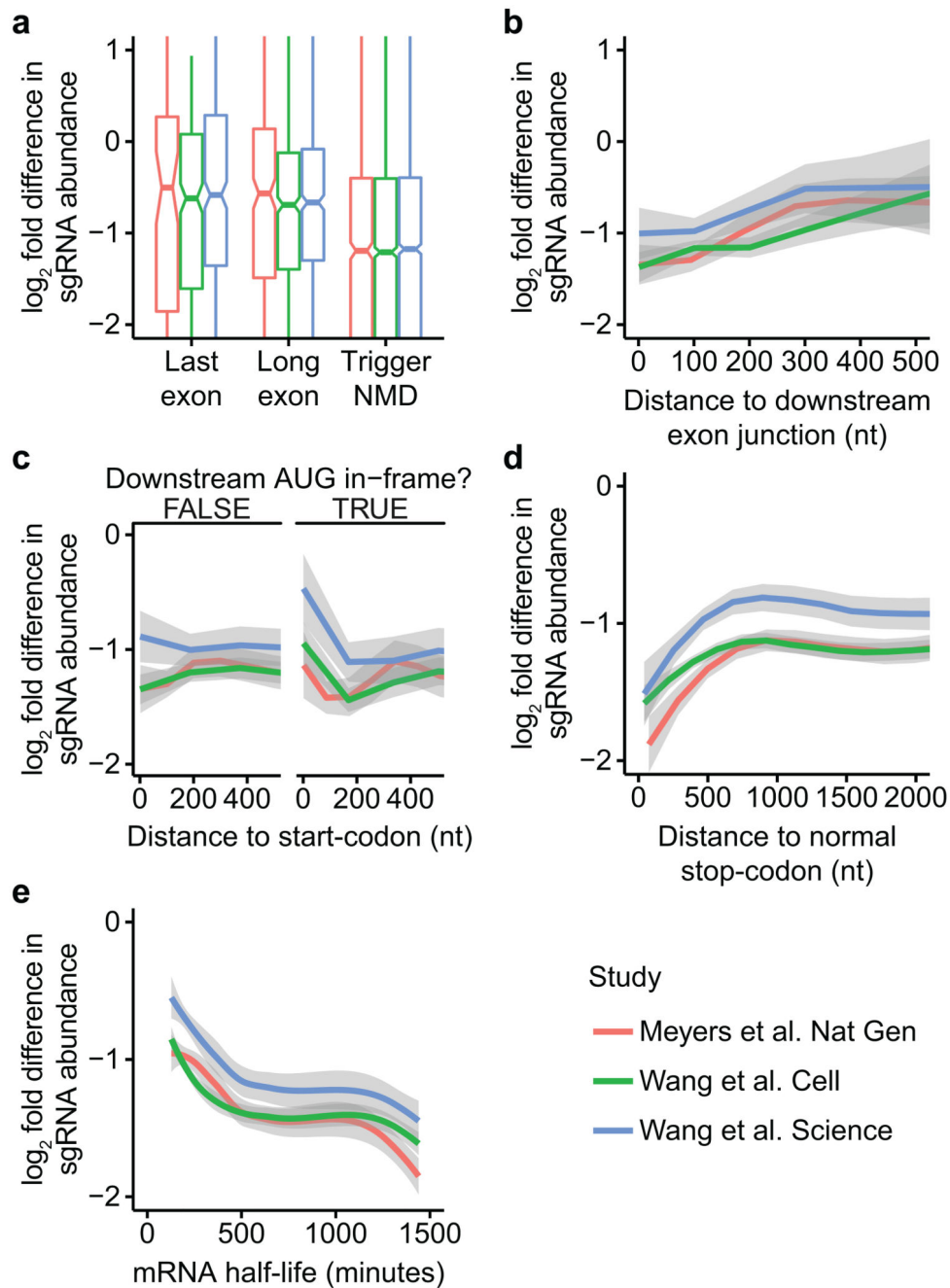
**a**, sgRNAs targeted to gene regions that evade NMD show a smaller enrichment when selecting for cells that do not express the targeted protein. Fold differences in sgRNA abundance are pooled per rule and shown for all proteins in **a** and additionally broken down by protein in **c**. P values are by Mann-Whitney U test, two-sided. **b**, Models that discriminate essential from non-essential genes based on the fold-depletion of sgRNAs are more accurate for sgRNAs that target gene regions that trigger NMD than for sgRNAs targeted to different NMD-evading regions.



**Extended Data Fig. 5. Relevance of NMD rules for CRISPR sgRNA design.**

**a**, fitness loss upon targeting a non-essential gene (left) versus an essential gene (right) using a sgRNA directed at gene sections which are covered by various NMD-evasion rules. **b-e**, distribution of loci targeted by sgRNAs that are NMD-detected or NMD-evading (according to the individual NMD rules) for genome-wide CRISPR libraries (**b, c**) or by sgRNA design tools (**d, e**).

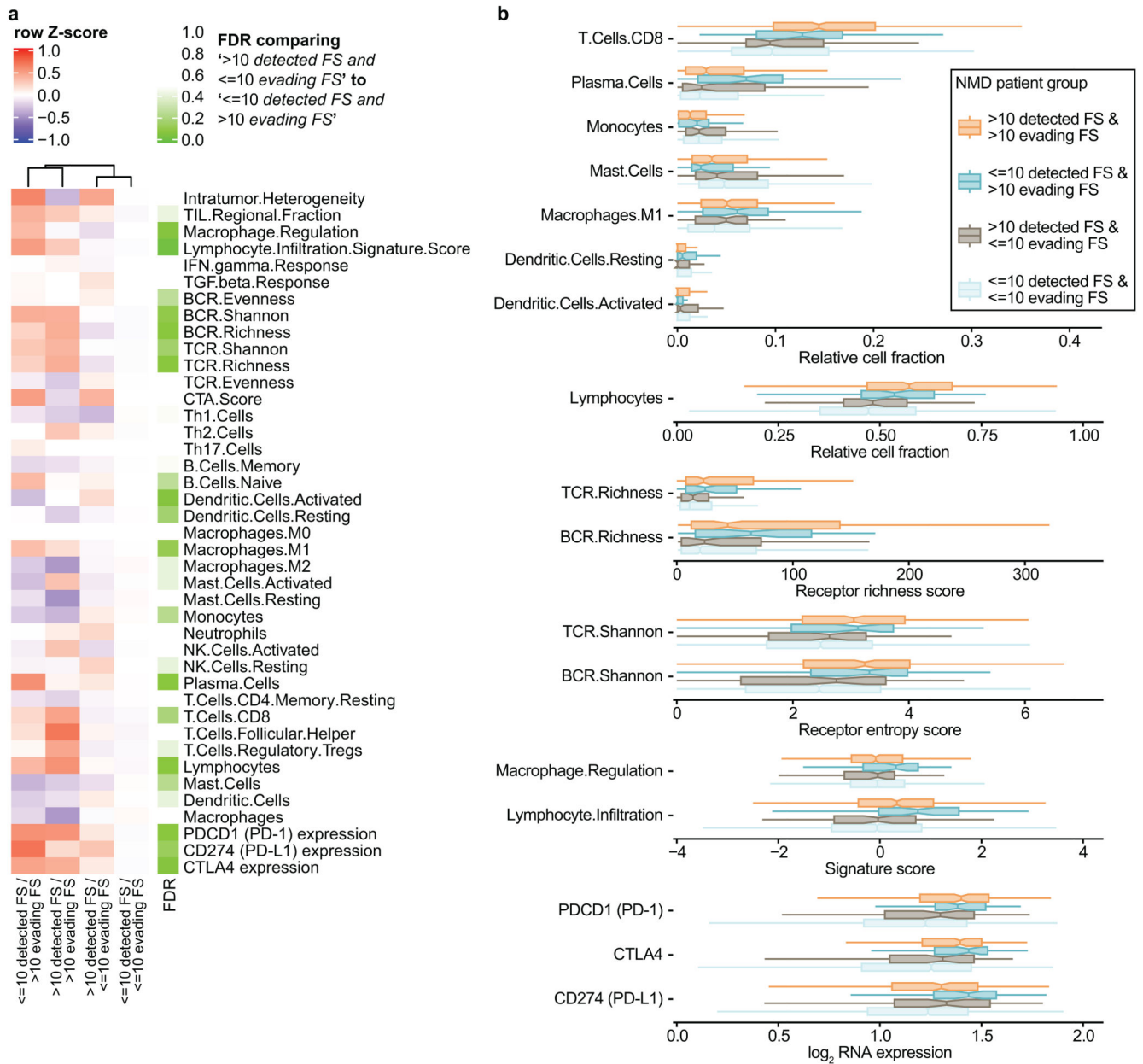




**Extended Data Fig.6. CRISPR screening data support canonical and non-canonical determinants of NMD efficacy.**

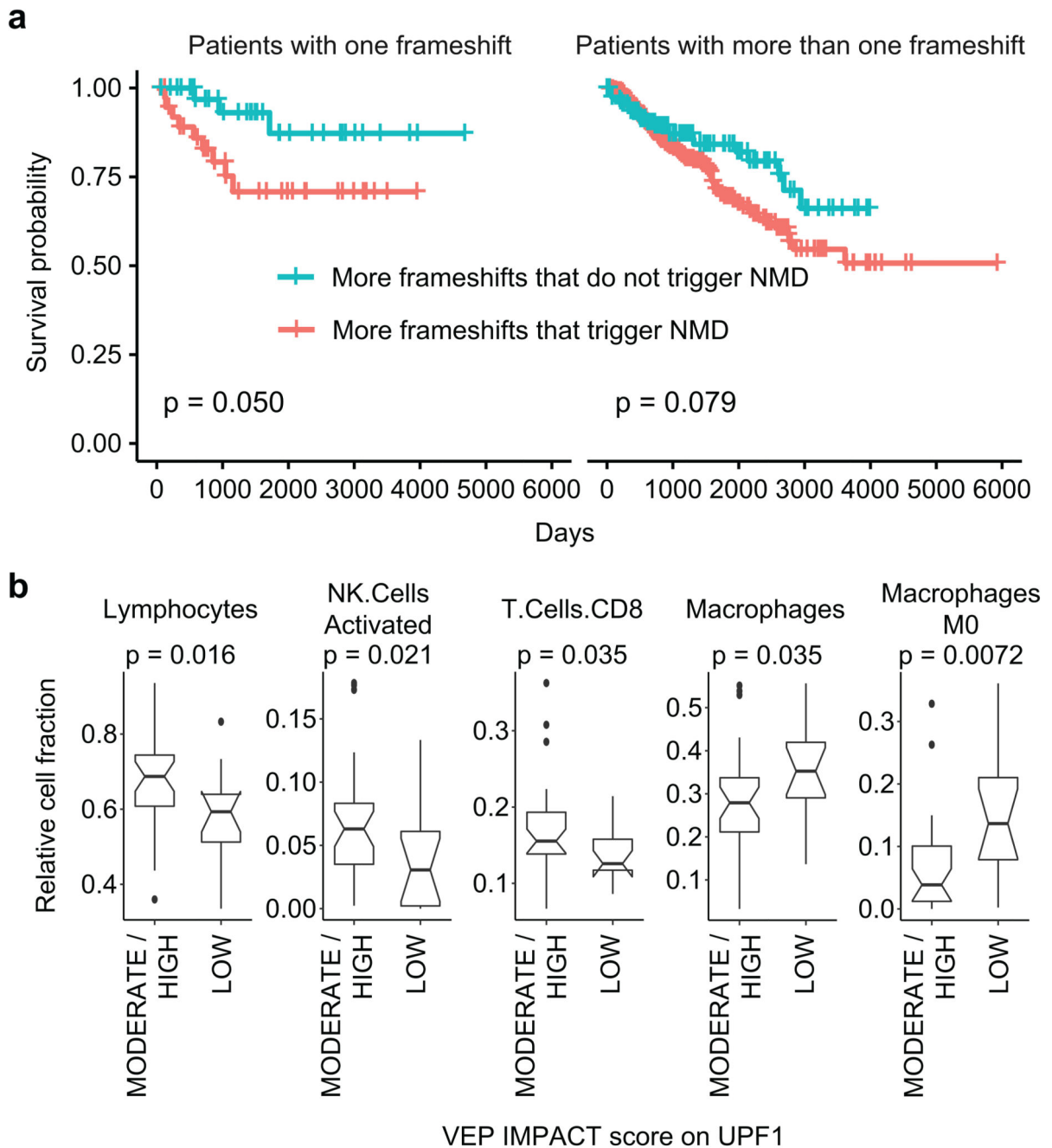
**a**, the non-canonical long-exon NMD evasion rule has similar effects as the canonical last-exon NMD evasion rule in terms of attenuated loss of fitness when targeting an essential gene (Methods). **b-e**, minor non-canonical NMD determinants, which are not included in the *NMDetective-B* model, but are included in the comprehensive *NMDetective-A* model. This includes: distance to downstream splice site in long exons (**b**), for the start-proximal rule, existence of a downstream in-frame AUG codon, presumably facilitating translation re-

initiation (**c**), distance to the *wild-type* stop codon (**d**), and the effect of mRNA turnover on the observed NMD efficacy (**e**).



**Extended Data Fig.7. Tumor infiltration by immune cells is associated with a high burden of NMD-evading frameshifting indels.**

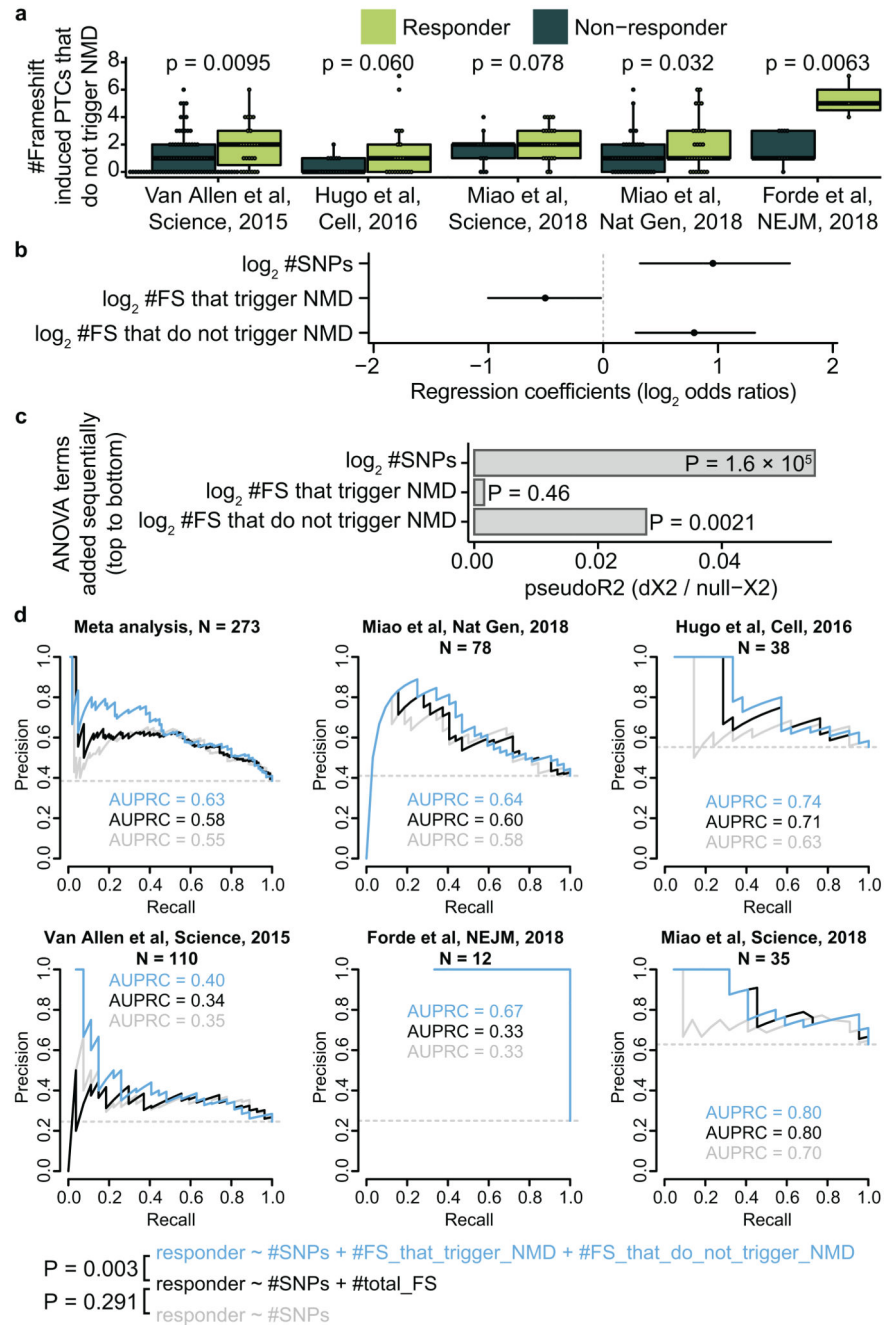
**a-b**, Individual immune markers for the TCGA samples were estimated using gene expression data<sup>50</sup>. FDR is by two-sided Mann-Whitney U test, Benjamini-Hochberg adjusted. In panel **b**, only tests significant at FDR<25% are shown.



**Extended Data Fig.8. Evidence that NMD activity is a determinant of immune reactivity of tumors.**

**a**, in the TCGA kidney cancer cohorts (KIRC, KICH and KIRP), a cancer type where indel burden is known to be particularly strongly associated with immunogenicity<sup>41</sup>, higher relative burden of NMD-evading frameshifts was associated with longer survival ( $p=0.011$  for pooled data from both panels, by log-rank test) without application of immunotherapy. Patients were separated based on the number of frameshifting indels that do not trigger NMD being higher than the number that trigger NMD (cyan) and those patients where the

converse is true (red). **b**, in the TCGA UCEC cohort of uterine corpus endometrial carcinoma, where the key NMD gene UPF1 is commonly mutated, the predicted higher impact of UPF1 mutations is associated with multiple gene-expression based markers of lymphocyte, but not macrophage, infiltration. Patients with more than one UPF1 mutation were assigned to the group of the mutation with the higher VEP score. P values by Mann-Whitney U test.



**Extended Data Fig.9. NMD rules improve predictions of response to immunotherapy across multiple cancer types.**

**a.** assigning NMD rules to frameshift mutations based on the location of the first downstream PTC in the new reading frame also shows that the burden of frameshifts that cannot trigger NMD is higher in patients that respond to immunotherapy. P values are by a one-tailed Mann-Whitney U test. **b.** standardized regression coefficients and the 95% confidence interval in a logistic regression model that predicts responders versus non-responders. **c.** pseudo- $R^2$  for sequential addition of features to a joint model. The null model



includes only the study (dataset) as a covariate. **d.** precision-recall curves for logistic regression models with three different sets of features: a tumor mutation burden (TMB) baseline, another baseline where TMB and all frameshifting indels are considered together, and the full model that considers TMB and NMD-evading and NMD-detected frameshifting indels separately. P values are by Chi-squared test. AUPRC, area under the precision-recall curve.

## Supplementary Material

Refer to Web version on PubMed Central for supplementary material.

## Acknowledgements

This work was funded by the ERC Starting Grant “HYPER-INSIGHT” (to F.S.) and the ERC Consolidator Grant “IR-DC” (to B.L.). R.L. and M.V. are supported by the Oncode Institute, which is partly funded by the Dutch Cancer Society (KWF), and M.V. also acknowledges support by the gravitation program CancerGenomiCs.nl from the Netherlands Organization for Scientific Research (NWO). F.S. and B.L. are funded by the ICREA Research Professor programme. F.S. and B.L. acknowledge support of the Severo Ochoa Centres of Excellence programme to the IRB Barcelona and to the CRG, respectively. B.L. and F.S. were supported by the Spanish Ministry of Economy and Competitiveness (BFU2017-89488-P and BFU2017-89833-P, respectively). B.L. was further supported by the Bettencourt Schueller Foundation, Agencia de Gestio d’Ajuts Universitaris i de Recerca (AGAUR, 2017 SGR 1322), and the CERCA Program/Generalitat de Catalunya. B.L. also acknowledges the support of the Spanish Ministry of Economy, Industry and Competitiveness (MEIC) to the EMBL partnership.

## References

1. Lykke-Andersen S, Jensen TH. Nonsense-mediated mRNA decay: an intricate machinery that shapes transcriptomes. *Nat Rev Mol Cell Biol.* 2015; 16:665–77. [PubMed: 26397022]
2. Popp MW, Maquat LE. Leveraging Rules of Nonsense-Mediated mRNA Decay for Genome Engineering and Personalized Medicine. *Cell.* 2016; 165:1319–1322. [PubMed: 27259145]
3. Silva AL, Romao L. The mammalian nonsense-mediated mRNA decay pathway: to decay or not to decay! Which players make the decision? *FEBS Lett.* 2009; 583:499–505. [PubMed: 19162024]
4. Nagy E, Maquat LE. A rule for termination-codon position within intron-containing genes: when nonsense affects RNA abundance. *Trends Biochem Sci.* 1998; 23:198–9. [PubMed: 9644970]
5. Le Hir H, Gatfield D, Izaurralde E, Moore MJ. The exon-exon junction complex provides a binding platform for factors involved in mRNA export and nonsense-mediated mRNA decay. *EMBO J.* 2001; 20:4987–97. [PubMed: 11532962]
6. Kashima I, et al. Binding of a novel SMG-1-Upf1-eRF1-eRF3 complex (SURF) to the exon junction complex triggers Upf1 phosphorylation and nonsense-mediated mRNA decay. *Genes Dev.* 2006; 20:355–67. [PubMed: 16452507]
7. Brogna S, Wen J. Nonsense-mediated mRNA decay (NMD) mechanisms. *Nat Struct Mol Biol.* 2009; 16:107–13. [PubMed: 19190664]
8. Rivas MA, et al. Human genomics. Effect of predicted protein-truncating genetic variants on the human transcriptome. *Science.* 2015; 348:666–9. [PubMed: 25954003]
9. Lindeboom RG, Supek F, Lehner B. The rules and impact of nonsense-mediated mRNA decay in human cancers. *Nat Genet.* 2016; 48:1112–8. [PubMed: 27618451]
10. Hu Z, Yau C, Ahmed AA. A pan-cancer genome-wide analysis reveals tumour dependencies by induction of nonsense-mediated decay. *Nat Commun.* 2017; 8:15943. [PubMed: 28649990]
11. Hoek TA, et al. Single-Molecule Imaging Uncovers Rules Governing Nonsense-Mediated mRNA Decay. *Mol Cell.* 2019
12. Miller JN, Pearce DA. Nonsense-mediated decay in genetic disease: friend or foe? *Mutat Res Rev Mutat Res.* 2014; 762:52–64. [PubMed: 25485595]
13. Khajavi M, Inoue K, Lupski JR. Nonsense-mediated mRNA decay modulates clinical outcome of genetic disease. *Eur J Hum Genet.* 2006; 14:1074–81. [PubMed: 16757948]

14. Coban-Akdemir Z, et al. Identifying Genes Whose Mutant Transcripts Cause Dominant Disease Traits by Potential Gain-of-Function Alleles. *The American Journal of Human Genetics*. 2018; 103:171–187. [PubMed: 30032986]
15. Mort M, Ivanov D, Cooper DN, Chuzhanova NA. A meta-analysis of nonsense mutations causing human genetic disease. *Hum Mutat*. 2008; 29:1037–47. [PubMed: 18454449]
16. Holbrook JA, Neu-Yilik G, Hentze MW, Kulozik AE. Nonsense-mediated decay approaches the clinic. *Nat Genet*. 2004; 36:801–8. [PubMed: 15284851]
17. Usuki F, et al. Inhibition of SMG-8, a subunit of SMG-1 kinase, ameliorates nonsense-mediated mRNA decay-exacerbated mutant phenotypes without cytotoxicity. *Proc Natl Acad Sci U S A*. 2013; 110:15037–42. [PubMed: 23983263]
18. Bokhari A, et al. Targeting nonsense-mediated mRNA decay in colorectal cancers with microsatellite instability. *Oncogenesis*. 2018; 7:70. [PubMed: 30228267]
19. Huang L, et al. Antisense suppression of the nonsense mediated decay factor Upf3b as a potential treatment for diseases caused by nonsense mutations. *Genome Biol*. 2018; 19:4. [PubMed: 29334995]
20. Lejeune F. Triple Effect of Nonsense-Mediated mRNA Decay Inhibition as a Therapeutic Approach for Cancer. *Single Cell Biol*. 2016; 5
21. Gorlov IP, Gorlova OY, Frazier ML, Spitz MR, Amos CI. Evolutionary evidence of the effect of rare variants on disease etiology. *Clin Genet*. 2011; 79:199–206. [PubMed: 20831747]
22. Maher MC, Uricchio LH, Torgerson DG, Hernandez RD. Population genetics of rare variants and complex diseases. *Hum Hered*. 2012; 74:118–28. [PubMed: 23594490]
23. Kerr TP, Sewry CA, Robb SA, Roberts RG. Long mutant dystrophins and variable phenotypes: evasion of nonsense-mediated decay? *Hum Genet*. 2001; 109:402–7. [PubMed: 11702221]
24. Hall GW, Thein S. Nonsense codon mutations in the terminal exon of the beta-globin gene are not associated with a reduction in beta-mRNA accumulation: a mechanism for the phenotype of dominant beta-thalassemia. *Blood*. 1994; 83:2031–7. [PubMed: 8161774]
25. Spinner NB, et al. Jagged1 mutations in alagille syndrome. *Hum Mutat*. 2001; 17:18–33. [PubMed: 11139239]
26. van Bon BW, et al. Intragenic deletion in DYRK1A leads to mental retardation and primary microcephaly. *Clin Genet*. 2011; 79:296–9. [PubMed: 21294719]
27. Brown LY, et al. Holoprosencephaly due to mutations in ZIC2: alanine tract expansion mutations may be caused by parental somatic recombination. *Hum Mol Genet*. 2001; 10:791–6. [PubMed: 11285244]
28. Banning A, Schiff M, Tikkanen R. Amlexanox provides a potential therapy for nonsense mutations in the lysosomal storage disorder Aspartylglucosaminuria. *Biochim Biophys Acta Mol Basis Dis*. 2018; 1864:668–675. [PubMed: 29247835]
29. Gonzalez-Hilarion S, et al. Rescue of nonsense mutations by amlexanox in human cells. *Orphanet J Rare Dis*. 2012; 7:58. [PubMed: 22938201]
30. Martin L, et al. Identification and characterization of small molecules that inhibit nonsense-mediated RNA decay and suppress nonsense p53 mutations. *Cancer Res*. 2014; 74:3104–13. [PubMed: 24662918]
31. Wang H, La Russa M, Qi LS. CRISPR/Cas9 in Genome Editing and Beyond. *Annu Rev Biochem*. 2016; 85:227–64. [PubMed: 27145843]
32. Wang T, et al. Identification and characterization of essential genes in the human genome. *Science*. 2015; 350:1096–101. [PubMed: 26472758]
33. Meyers RM, et al. Computational correction of copy number effect improves specificity of CRISPR-Cas9 essentiality screens in cancer cells. *Nat Genet*. 2017; 49:1779–1784. [PubMed: 29083409]
34. Wang T, et al. Gene Essentiality Profiling Reveals Gene Networks and Synthetic Lethal Interactions with Oncogenic Ras. *Cell*. 2017; 168:890–903 e15. [PubMed: 28162770]
35. Findlay GM, et al. Accurate classification of BRCA1 variants with saturation genome editing. *Nature*. 2018; 562:217–222. [PubMed: 30209399]

36. Doench JG, et al. Rational design of highly active sgRNAs for CRISPR-Cas9-mediated gene inactivation. *Nat Biotechnol.* 2014; 32:1262–7. [PubMed: 25184501]
37. Allen F, et al. Predicting the mutations generated by repair of Cas9-induced double-strand breaks. *Nat Biotechnol.* 2018
38. Hargadon KM, Johnson CE, Williams CJ. Immune checkpoint blockade therapy for cancer: An overview of FDA-approved immune checkpoint inhibitors. *Int Immunopharmacol.* 2018; 62:29–39. [PubMed: 29990692]
39. Chalmers ZR, et al. Analysis of 100,000 human cancer genomes reveals the landscape of tumor mutational burden. *Genome Med.* 2017; 9:34. [PubMed: 28420421]
40. Goodman AM, et al. Tumor Mutational Burden as an Independent Predictor of Response to Immunotherapy in Diverse Cancers. *Mol Cancer Ther.* 2017; 16:2598–2608. [PubMed: 28835386]
41. Turajlic S, et al. Insertion-and-deletion-derived tumour-specific neoantigens and the immunogenic phenotype: a pan-cancer analysis. *Lancet Oncol.* 2017; 18:1009–1021. [PubMed: 28694034]
42. Van Allen EM, et al. Genomic correlates of response to CTLA-4 blockade in metastatic melanoma. *Science.* 2015; 350:207–211. [PubMed: 26359337]
43. Hugo W, et al. Genomic and Transcriptomic Features of Response to Anti-PD-1 Therapy in Metastatic Melanoma. *Cell.* 2016; 165:35–44. [PubMed: 26997480]
44. Miao D, et al. Genomic correlates of response to immune checkpoint therapies in clear cell renal cell carcinoma. *Science.* 2018; 359:801–806. [PubMed: 29301960]
45. Forde PM, et al. Neoadjuvant PD-1 Blockade in Resectable Lung Cancer. *N Engl J Med.* 2018; 378:1976–1986. [PubMed: 29658848]
46. Miao D, et al. Genomic correlates of response to immune checkpoint blockade in microsatellite-stable solid tumors. *Nat Genet.* 2018; 50:1271–1281. [PubMed: 30150660]
47. Durand S, et al. Inhibition of nonsense-mediated mRNA decay (NMD) by a new chemical molecule reveals the dynamic of NMD factors in P-bodies. *J Cell Biol.* 2007; 178:1145–60. [PubMed: 17893241]
48. Keeling KM, et al. Attenuation of nonsense-mediated mRNA decay enhances in vivo nonsense suppression. *PLoS One.* 2013; 8:e60478. [PubMed: 23593225]
49. Pastor F, Kolonias D, Giangrande PH, Gilboa E. Induction of tumour immunity by targeted inhibition of nonsense-mediated mRNA decay. *Nature.* 2010; 465:227–30. [PubMed: 20463739]
50. Gonzalez-Porta M, Frankish A, Rung J, Harrow J, Brazma A. Transcriptome analysis of human tissues and cell lines reveals one dominant transcript per gene. *Genome Biol.* 2013; 14:R70. [PubMed: 23815980]
51. Grossman RL, et al. Toward a Shared Vision for Cancer Genomic Data. *N Engl J Med.* 2016; 375:1109–12. [PubMed: 27653561]
52. Friedel CC, Dolken L, Ruzsics Z, Koszinowski UH, Zimmer R. Conserved principles of mammalian transcriptional regulation revealed by RNA half-life. *Nucleic Acids Res.* 2009; 37:e115. [PubMed: 19561200]
53. Haeussler M, et al. The UCSC Genome Browser database: 2019 update. *Nucleic Acids Res.* 2019; 47:D853–D858. [PubMed: 30407534]
54. Lek M, et al. Analysis of protein-coding genetic variation in 60,706 humans. *Nature.* 2016; 536:285–91. [PubMed: 27535533]
55. Landrum MJ, et al. ClinVar: improving access to variant interpretations and supporting evidence. *Nucleic Acids Res.* 2018; 46:D1062–D1067. [PubMed: 29165669]
56. Balasubramanian S, et al. Using ALoFT to determine the impact of putative loss-of-function variants in protein-coding genes. *Nat Commun.* 2017; 8:382. [PubMed: 28851873]
57. Karczewski KJ, et al. Variation across 141,456 human exomes and genomes reveals the spectrum of loss-of-function intolerance across human protein-coding genes. *bioRxiv.* 2019
58. Hart T, Moffat J. BAGEL: a computational framework for identifying essential genes from pooled library screens. *BMC Bioinformatics.* 2016; 17:164. [PubMed: 27083490]
59. Altschul SF, Gish W, Miller W, Myers EW, Lipman DJ. Basic local alignment search tool. *J Mol Biol.* 1990; 215:403–10. [PubMed: 2231712]

60. Heigwer F, Kerr G, Boutros M. E-CRISP: fast CRISPR target site identification. *Nat Methods*. 2014; 11:122–3. [PubMed: 24481216]
61. Thorsson V, et al. The Immune Landscape of Cancer. *Immunity*. 2018; 48:812–830 e14. [PubMed: 29628290]
62. Eisenhauer EA, et al. New response evaluation criteria in solid tumours: revised RECIST guideline (version 1.1). *Eur J Cancer*. 2009; 45:228–47. [PubMed: 19097774]
63. Wolchok JD, et al. Guidelines for the evaluation of immune therapy activity in solid tumors: immune-related response criteria. *Clin Cancer Res*. 2009; 15:7412–20. [PubMed: 19934295]

### Editorial Summary

The authors explore the impact of nonsense-mediated mRNA decay (NMD) on human genetic disease and cancer immunotherapy by applying the rules of NMD genome-wide as a resource called NMDetective.

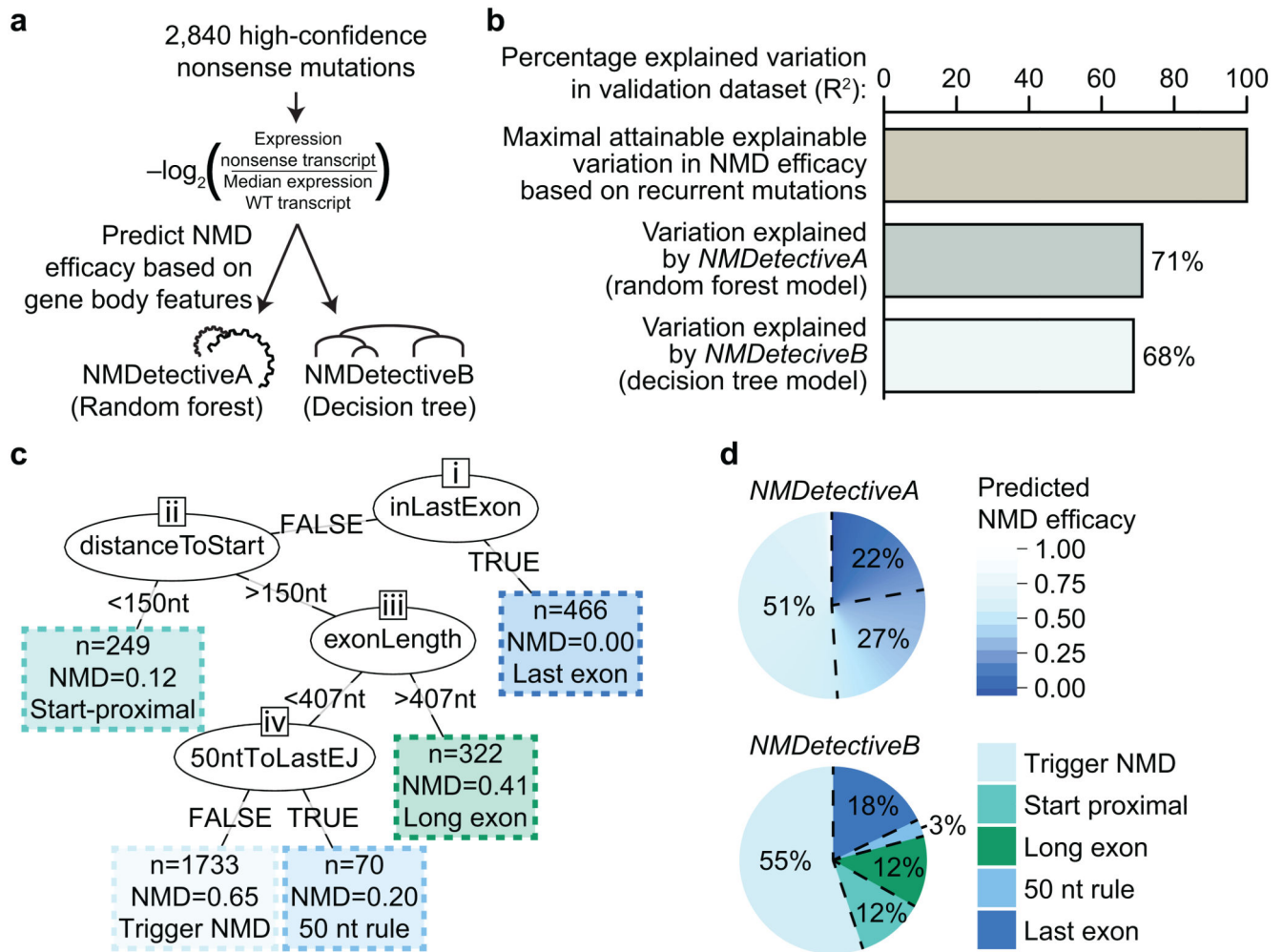


**Figure 1. *NMDetective* catalogues the effects of all possible PTCs in the human genome.**

**a**, an overview of the data used to create the *NMDetective-A* and *-B* resources. **b**, accuracy of predictions by *NMDetective* evaluated on an independent set of frameshifting indel mutations. **c**, the *NMDetective-B* decision tree model. The number of PTCs in the training set assigned to each group is shown as *n*. **d**, coverage of the gene coding regions with NMD rules.



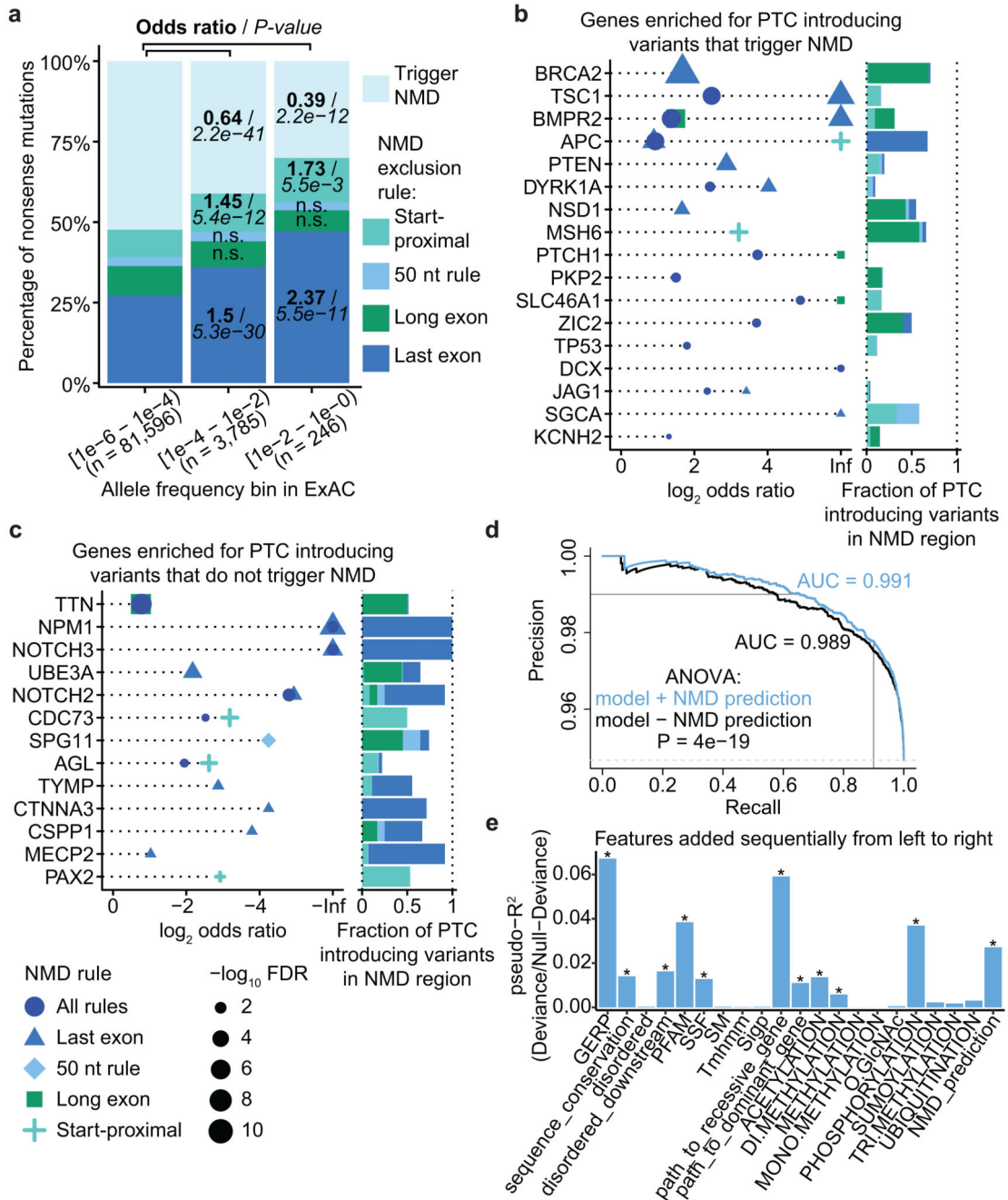


**Figure 2. Disease phenotypes arising from germline PTCs are modulated by NMD.** **a**, signatures of negative selection on NMD-detected variants in population genomic data. **b**, genes where NMD is predicted to aggravate the phenotype, **c**, genes where NMD is predicted to alleviate the phenotype. **b-c**, genes significant at an FDR<5% are shown (see Extended Data Fig. 3c-d for a more permissive list at FDR<25%).  $\log_2$  odds ratios are for ClinVar frequencies of frameshifting indel and nonsense variants in NMD-evading versus NMD-detected regions of a gene, normalized to the length of the regions. FDRs are by a Fisher’s exact test, two-tailed, Benjamini-Hochberg adjusted. **d**, NMD rules significantly



improve predictions of PTC pathogenicity, **e.** variable importance in the PTC pathogenicity predictor, \* significant at  $p < 0.001$  by Chi-Square-test.

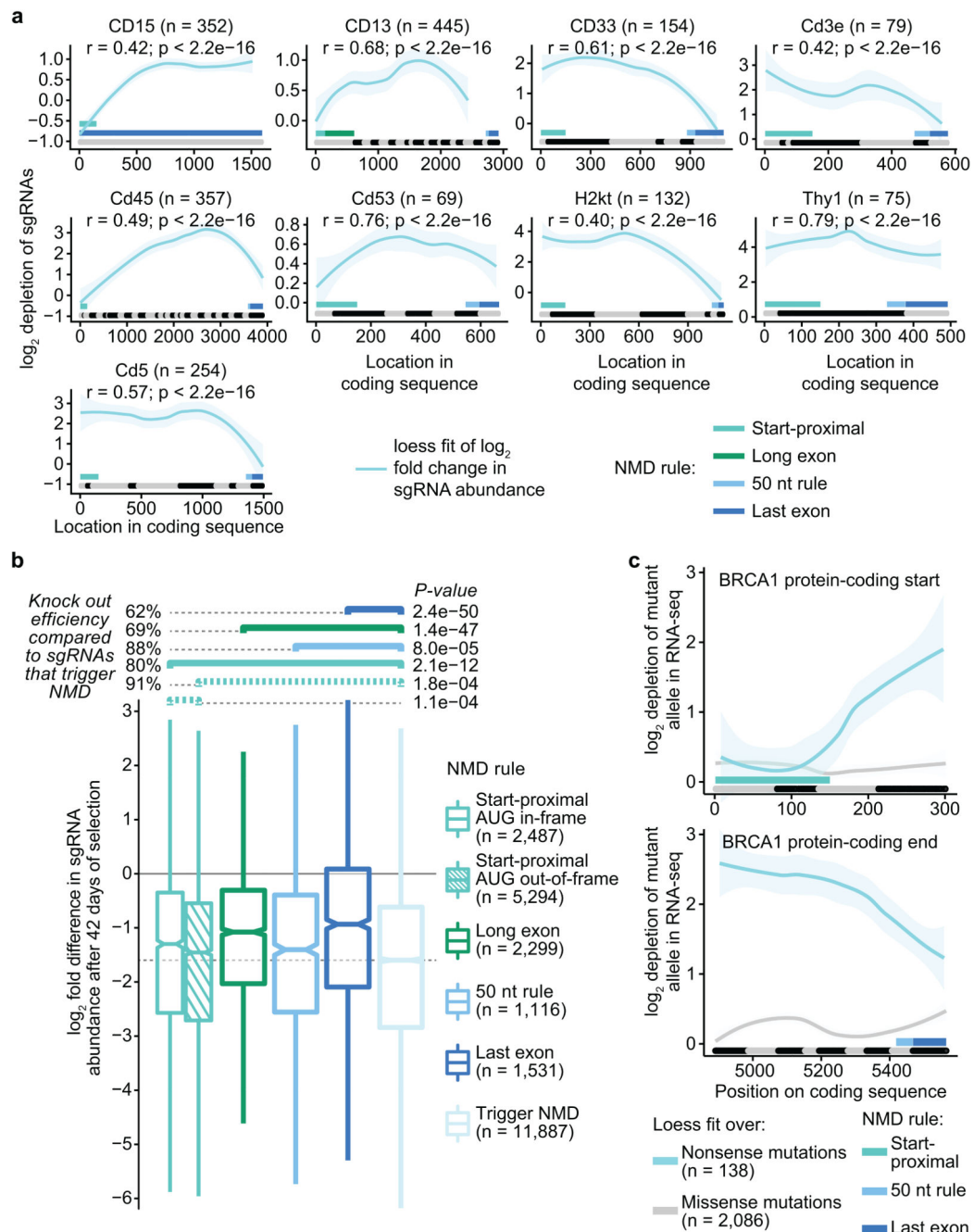


**Figure 3. NMD rules determine the outcome of CRISPR-Cas9 gene editing.**

**a**, a decrease in protein expression due to tiling sgRNAs placed along the length of human and mouse genes (y axis quantifies the sgRNA fold difference between a low-expressing versus high-expressing set of cells) reveals, overall, similar associations with the non-canonical start-proximal NMD rule to the canonical NMD last-exon rule. The CD13 gene demonstrates the effect of the non-canonical long-exon rule. Shaded regions are 95% confidence interval of the *loess* fit to protein expression. Pearson correlation coefficients and two-sided tests for association were computed by comparing the loess fit to the

*NMDetective*-A NMD efficacy scores. **b**, evading NMD attenuates the loss of fitness (y axis) due to knockout of essential genes. Data for non-essential genes are in Extended Data Fig. 5a. P values are by Mann-Whitney U test. The knock-out efficiency compares the reduction of sgRNAs in NMD evading regions to the reduction in regions that trigger NMD. **c**, a ‘saturation genome editing’ CRISPR experiment shows strongly reduced mRNA levels for nonsense mutations in BRCA1, except for those introduced into regions covered by the start-proximal (top) and last-exon NMD evasion rules (bottom panel).

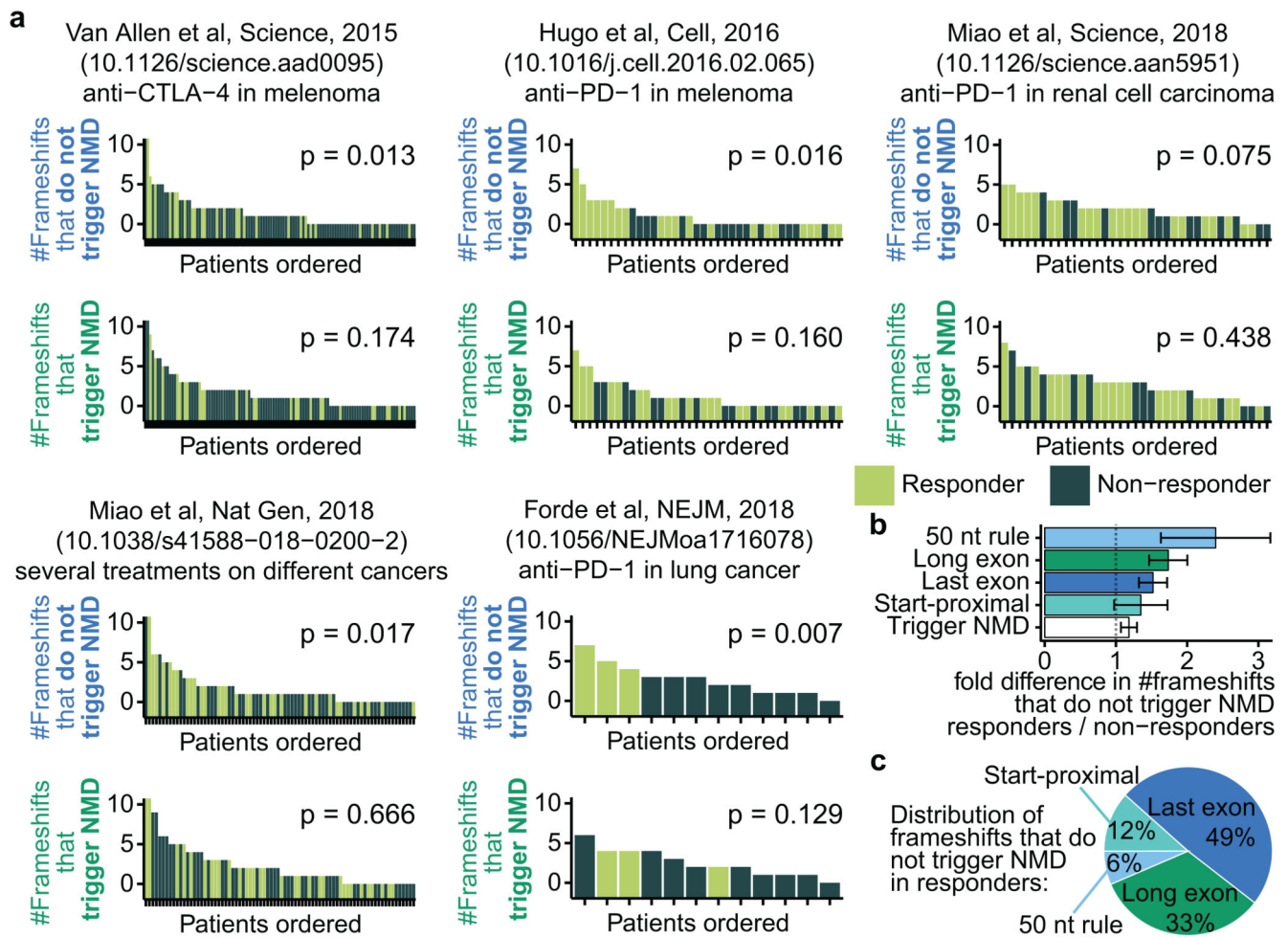


**Figure 4. Efficacy of immunotherapy is predicted by the burden of NMD-evading frameshifting indels but not other indels.**

**a**, across five studies, responders to immune checkpoint blockade are enriched for a high burden of NMD-evading (top panels) but not for NMD-detected (bottom panels) frameshifting indels. P values are by Mann-Whitney U test (one-tailed, testing positive association of responders with higher burden). **b**, enrichment for NMD-evading frameshifting indels in responders *versus* non-responders is observed for all four NMD rules. Error bars are 95% confidence intervals, **c**, coverage of NMD-evading frameshifting indels by the individual NMD rules, observed in exomes of immunotherapy responders.